





# Searching in HI for Massive Low Surface Brightness Galaxies: Samples from HyperLeda and the UGC

K. O’Neil<sup>1</sup> , Stephen E. Schneider<sup>2</sup>, W. van Driel<sup>3,4</sup> , G. Liu<sup>2</sup>, T. Joseph<sup>5,6</sup>, A. C. Schwortz<sup>2,7</sup>, and Z. Butcher<sup>2,8</sup>

<sup>1</sup>Green Bank Observatory, 155 Observatory Road, Green Bank, WV 24934, USA; [koneil@nrao.edu](mailto:koneil@nrao.edu)

<sup>2</sup>University of Massachusetts, Astronomy Program, 536 LGRC, Amherst, MA 01003, USA

<sup>3</sup>GEPI, Observatoire de Paris, Université PSL, CNRS, 5 place Jules Janssen, 92195 Meudon, France

<sup>4</sup>Observatoire Radioastronomique de Nançay, Observatoire de Paris, Université PSL, Université d’Orléans, 18330 Nançay, France

<sup>5</sup>Astrophysics, Cosmology and Gravity Centre (ACGC), Department of Astronomy, University of Cape Town, Private Bag X3, Rondebosch 7701, South Africa

<sup>6</sup>Anton Pannekoek Institute for Astronomy, Faculty of Science, University of Amsterdam, Science Park 904, 1098 XH Amsterdam, The Netherlands

<sup>7</sup>Quinsigamond Community College, 670 W Boylston Street, Box 224, Worcester, MA 01606-2092, USA

<sup>8</sup>National Radio Astronomy Observatory, 520 Edgemont Road, Charlottesville, VA 22903, USA

Received 2023 February 2; revised 2023 April 24; accepted 2023 April 30; published 2023 June 1

## Abstract

A search has been made for 21 cm HI line emission in a total of 350 unique galaxies from two samples whose optical properties indicate they may be massive. The first consists of 241 low surface brightness (LSB) galaxies of morphological type Sb and later selected from the HyperLeda database and the second consists of 119 LSB galaxies from the UGC with morphological types Sd-m and later. Of the 350 unique galaxies, 239 were observed at the Nançay Radio Telescope, 161 at the Green Bank Telescope, and 66 at the Arecibo telescope. A total of 295 (84.3%) were detected, of which 253 (72.3%) appear to be uncontaminated by any other galaxies within the telescope beam. Finally, of the total detected, uncontaminated galaxies, at least 31 appear to be massive LSB galaxies, with a total HI mass  $\geq 10^{10} M_{\odot}$ , for  $H_0 = 70 \text{ km s}^{-1} \text{ Mpc}^{-1}$ . If we expand the definition to also include galaxies with significant total (rather than just gas) mass, i.e., those with an inclination-corrected HI line width  $W_{50,\text{cor}} > 500 \text{ km s}^{-1}$ , this brings the total number of massive LSB galaxies to 41. There are no obvious trends between the various measured global galaxy properties, particularly between mean surface brightness and galaxy mass.

*Unified Astronomy Thesaurus concepts:* Amorphous irregular galaxies (37); Radio astronomy (1338); Spiral galaxies (1560); Low surface brightness galaxies (940)

*Supporting material:* figure set, machine-readable tables

## 1. Introduction

Low surface brightness (LSB) galaxies—spiral galaxies with a central surface brightness at least 1 mag arcsec<sup>-2</sup> fainter than the night sky—are now well established as a class of galaxies with properties distinct from the high surface brightness (HSB) objects that define the Hubble sequence. However, considerable uncertainty still exists about the range of LSB galaxy properties and their number density in the  $z \leq 0.1$  universe. As LSB galaxies encompass many of the extremes in galaxy properties, gaining a firm understanding of their properties and number counts is vital for testing galaxy formation and evolution theories, as well as for determining the relative amounts of baryons that are contained in galaxy potentials, compared to those that may comprise the intergalactic medium. As we will show, we have not yet fully sampled the LSB galaxy parameter space. In addition, it should be emphasized that there may still be large numbers of LSB galaxies with properties beyond our present detection limits.

The traditional (albeit erroneous) perception of LSB galaxies is that they are young dwarf galaxies which have undergone little star formation: low-mass, late-type, fairly blue systems with relatively high  $M_{\text{HI}}/L_{\text{B}}$  ratios and low metallicities. In practice, however, LSB disk galaxies are known to have a remarkable

diversity in properties, including very red objects with near-solar metallicity (e.g., O’Neil et al. 2007), as well as massive ( $M_{\text{HI}} \geq 10^{10} M_{\odot}$ , for  $H_0 = 70 \text{ km s}^{-1} \text{ Mpc}^{-1}$ ) systems such as Malin 1 (the largest disk galaxy found to date), [SII93] 1226+010, Malin 2, and others (e.g., Bothun et al. 1987; Sprayberry et al. 1995). Note, too, that the galaxies’ observed HI richness may be biased by the fact that their redshifts are often determined through HI observations—an optical redshift survey of LSB galaxies observed at 21 cm (Burkholder et al. 2001) also contains objects with very-low  $M_{\text{HI}}/L_{\text{B}}$  ratios (Bell & Bower 2000).

In principle, massive, or giant, LSB galaxies can be defined by different criteria. Based on surface photometry, Sprayberry et al. (1995) defined a “diffuseness index” to distinguish massive LSB galaxies, which is based on the deprojected blue central surface brightness  $\mu_{\text{B}}(0)$  and the scale length of the disk  $h_r$ —the seven giants in their paper have  $\langle \mu_{\text{B}} \rangle = 23.2 \text{ mag arcsec}^{-2}$  and  $\langle h_r \rangle = 13.0 \text{ kpc}$ . Other selection criteria can be used as well, such as the deprojected central blue disk surface brightness  $\mu_{\text{B}}(0) \geq 23 \text{ mag arcsec}^{-2}$ , HI mass  $M_{\text{HI}} \geq 10^{9.5-10} M_{\odot}$ , or optical diameter  $\geq 50 \text{ kpc}$  (e.g., Pickering et al. 1997; Mishra et al. 2017; Kulier et al. 2020). In the present study we use the criterion  $M_{\text{HI}} \geq 10^{10} M_{\odot}$  to identify massive galaxies, although we also consider the cases with high dynamical mass as defined by an inclination-corrected line width  $W_{50,\text{cor}} \geq 500 \text{ km s}^{-1}$ .

Massive LSB galaxies are interesting for a number of reasons:

1. The current rate and history of star formation in massive LSB galaxies is puzzling. Optical photometry shows that



Original content from this work may be used under the terms of the [Creative Commons Attribution 4.0 licence](https://creativecommons.org/licenses/by/4.0/). Any further distribution of this work must maintain attribution to the author(s) and the title of the work, journal citation and DOI.

**Table 1**  
Literature Values—Optical Properties and Known Velocities for All Galaxies

Name	R.A. (J2000.0)	Decl. (J2000.0)	Morph.	$B_T$ (mag)	D25 ( $''$ )	b/a	$V_{\text{opt}}$ ( $\text{km s}^{-1}$ )	Opt. ref.	$V_{\text{HI}}$ ( $\text{km s}^{-1}$ )	HI reference
HI detections										
ESO 300-020	03 14 07.0	−37 59 29	(dIAB(s)m?)	17.27	0.50	0.54				
ESO 338-020	19 41 17.0	−38 12 49	Sbc	17.08	0.62	0.45				
ESO 346-034	23 10 00.0	−37 20 01	(dwarf)	16.42	0.69	0.49				
ESO 359-009	03 54 59.0	−35 47 21	Sbc	16.52	0.79	0.48				
ESO 368-004	07 32 54.0	−35 29 19	I	16.49	0.91	0.63			1397	<a href="#">Sta16</a>
ESO 371-004	08 40 14.0	−32 55 49	Sbc	16.18	0.56	0.49				
ESO 371-007	08 41 16.0	−33 15 53	Sbc	16.09	0.42	0.56				
ESO 371-017	08 48 16.0	−33 49 16	SBm	16.11	0.63	0.34				
ESO 377-005	11 05 37.0	−36 33 39	SBbc	16.12	0.55	0.60				
ESO 377-045	11 25 46.0	−36 48 36	Sbc	16.77	0.63	0.65			3087	<a href="#">Mta96</a>
...										
Spurious HI detections										
CGMW 1-0409	06 49 39.0	−14 24 36			0.41	1.00			2802	<a href="#">Rya02</a>
PGC 3995805	07 49 33.0	+39 44 24	I	17.38	0.54	0.78	2943	<a href="#">DR13</a>		
UGC 2305	02 49 37.9	+38 15 41	dw	18.00	0.90	0.42				
...										
HI nondetections										
ESO 366-014	06 43 53.0	−37 07 46	Sa	15.53	1.00	0.26	9229	<a href="#">Huc12</a>		
ESO 435-001	09 50 05.0	−29 25 30	(N)	14.88	0.51	0.54	1164	6dF		
ESO 491-002	06 50 37.0	−23 22 47	Sbc	16.31	1.07	0.38				
...										
Target galaxies outside the HI search range										
UGC 4879	09 16 03.3	+52 50 29	Iam	13.80	2.10	0.62	−25	<a href="#">Bel11b</a>	−86	<a href="#">Bel11b</a>
UGC 5442	10 07 01.7	+67 49 37	Im:	16.70	1.70	0.89	−17	<a href="#">Sim02</a>		
UGC 5692	10 30 34.6	+70 37 13	Sm:	11.60	3.50	0.85	56	<a href="#">Mak03</a>		
...										

**Note.** In the case more than one type of velocity is given, the references are listed in order. In the case more than one velocity of a given type is found in the literature, the most recent value is listed. Velocity references: 6dF—Jones et al. (2009); Bel11a—Bellazzini et al. (2011a); Bel11b—Bellazzini et al. (2011b); Ber02—Berrington et al. (2002) Bil14—Bilicki et al. (2014); Bou09—Bouchard et al. (2009); Bra03—Braun et al. (2003); Bra17—Bralts-Kelly et al. (2017); Dab16—Dabringhausen & Fellhauer (2016); Col01—Collless et al. (2001); Cou09—Courtois et al. (2009); DR4—Abazajian et al. (2004); DR5—Adelman-McCarthy et al. (2007); DR7—Abazajian et al. (2009); DR9—Ahn et al. (2012); DR12—Alam et al. (2015); DR13—Albareti et al. (2017); Fal99—Falco et al. (1999); Geh17—Geha et al. (2017); Hay18—Haynes et al. (2018); Huc01—Huchtmeier et al. (2001); Huc12—Huchra et al. (2012); Huc83—Huchra et al. (1983); Huc99—Huchra et al. (1999); Imp96—Impey et al. (1996); Imp01—Impey et al. (2001); Jon05—Jones et al. (2005); Jon09—Jones et al. (2009); Kar13—Karachentsev et al. (2013); Kar84—Karachentsev & Karachentseva (1984); Kaz02—Kazarian & Karapetian (2002); Kou17—Kourkchi & Tully (2017); Mak01—Makarov et al. (2001); Mak03—Makarov et al. (2003); Mak97—Makarov et al. (1997); Mar96—Marzke et al. (1996); Mas14—Masters et al. (2014); Mat00—Matthews & van Driel (2000); Mat96—Matthews & Gallagher (1996); Mey04—Meyer et al. (2004); Mon03—Monnier Ragainie et al. (2003a); NED—Ned Team (1992); Pat03—Paturel et al. (2003); Pro08—Proctor et al. (2008); Ram16—Ramatsoku et al. (2016); Rin00—Rines et al. (2000); Rin03—Rines et al. (2003); Rin16—Rines et al. (2016); Rya02—Ryan-Weber et al. (2002); Sim02—Simien & Prugniel (2002); Spr05—Springob et al. (2005); Ste84—Stetson (1984); Sta16—Staveley-Smith et al. (2016); Str88—Strauss & Davis (1988); The05—Theureau et al. (2005); The98—Theureau et al. (1998); Van16—van Driel et al. (2016); Ver06—Véron-Cetty et al. (2006); War07—Warren et al. (2007); Zab98—Zabludoff & Mulchaey (1998).

(This table is available in its entirety in machine-readable form.)

most have blue colors, and this appears to be due in part to lower metallicities, as well as to a young population of stars (e.g., O’Neil et al. 1997). What has delayed star formation in such massive galaxies?

- How the massive LSB galaxies have evolved into large disk systems without converting much of their gas into stars poses an interesting problem for galaxy evolution models. Are they in environments where the disks have remained undisturbed, are they all in the late stage of mergers, have they only recently been assembled, or does their high dark matter content play a role in their stellar evolution (Pickering et al. 1997; van den Hoek et al. 2000; Lelli et al. 2010; Galaz et al. 2011; Du et al. 2015)?
- Much of the HI in the local universe is tied up in LSBs, either in dwarfs (which constitute the great majority of LSBs) or in higher-mass galaxies that have large HI-to-

optical flux ratios (Rosenberg & Schneider 2002). Massive LSBs are rare, but can contain very large HI masses. What is their overall contribution to the HI mass function?

- Finally, massive LSB galaxies often have a significant bulge component, and frequently an active nucleus, raising the question of how the extremely large and extremely diffuse stellar disks of many of these objects continue to exist (e.g., Gallagher & Bushouse 1983; Knezek 1993; Schombert 1998; Knezek et al. 1999).

The origin and evolutionary histories of massive LSB galaxies remain unclear. Hoffman et al. (1992) proposed a scenario with giants forming from rare, low-density fluctuations in very-low-density regions, which should give rise to quiescent, gas-rich disks, with flat rotation curves with  $v_{\text{max}} \sim 300 \text{ km s}^{-1}$ . Knezek (1993) suggested an alternative scenario, based on

**Table 2**  
HI Results: Average HI Values for All Detections

Name	Sample	Notes	Conf.	$V_{\text{HI}}$	Error ( $\text{km s}^{-1}$ )	$W_{50}$	$W_{50,\text{cor}}$ ( $\text{km s}^{-1}$ )	$W_{20}$	rms mJy	Flux ( $\text{Jy km s}^{-1}$ )	Error	$\text{Log}(M_{\text{HI}}/M_{\odot})$	Error	Tel.
CGMW 1-0409	HLS	Y	1	2805	1	132	177	147	1.70	8.59	0.19	9.51	0.01	G
ESO 300-020	HL	N	1	13256	5	81	110	85	1.46	0.22	0.10	9.27	0.20	G
ESO 338-020	HL	Y	3	6377	6	379	438	396	4.11	3.88	0.76	9.88	0.09	N
ESO 346-034	HL	N	1	1805	14	58	80	107	1.60	0.89	0.16	8.12	0.08	G
ESO 359-009	HL	N	1	5850	7	221	265	247	4.08	3.24	0.44	9.72	0.06	N
ESO 368-004	HL	Y	1	1397	2	77	114	95	4.08	13.98	0.12	9.07	0.00	NGG
ESO 371-004	HL	N	1	1393	4	74	98	102	4.11	3.18	0.29	8.43	0.04	N
ESO 371-007	HL	N	1	2454	3	132	173	150	4.16	3.28	0.35	8.98	0.05	N
ESO 371-017	HL	N	1	1604	5	175	200	189	1.86	0.83	0.24	7.98	0.12	N
ESO 377-005	HL	N	1	2519	5	45	70	65	4.96	1.29	0.28	8.57	0.09	N
ESO 377-045	HL	Y	1	3125	16	108	156	171	4.48	2.44	0.41	9.05	0.07	N
ESO 385-016	HL	N	1	8283	32	139	176	214	3.63	1.61	0.49	9.72	0.13	N
...							...							...

(This table is available in its entirety in machine-readable form.)

Kormendy & Westpfahl (1989), whereby LSB giants may have dissipatively formed from massive, metal-poor dark matter halos. More recent studies have expounded on these, theorizing that LSB galaxies start as an HSB disk galaxy (Saburova et al. 2021) or spheroid (Clauwens et al. 2018) with the LSB disk forming later through the accretion of external gas. Another possibility is that they form through the merger of more than one galaxy (e.g., Martin et al. 2019) and/or that the disk itself is the result of a recent merger and will eventually coalesce into an HSB disk (e.g., Zavala et al. 2016; Clauwens et al. 2018). Finally, of course, it is possible that all of these scenarios are correct in different circumstances, and that the evolutionary histories of massive LSB galaxies are as complex as those of their HSB counterparts (e.g., Kulier et al. 2020). However, the limited number of objects available for study makes testing these theories challenging, at best.

We have previously undertaken surveys to explore the number density and HI properties of massive LSB galaxies in the nearby universe. These earlier projects focused on two different samples—late-type LSB galaxies found in the Uppsala General Catalogue of Galaxies (UGC; Nilson 1973; O’Neil et al. 2004) and near-infrared LSB galaxies found in the Two Micron All Sky Survey (2MASS) catalog (Monnier Ragaigine et al. 2003a, 2003b, 2003c). Both samples were observed in HI using the Nançay and Arecibo radio telescopes with good success: out of 231 UGC galaxies observed, 146 were detected, including 47 (32% of the detected objects) massive LSB galaxies, and out of the 701 2MASS galaxies observed, 278 were detected, of which 31 (11%) were also found to be massive. These results established that massive LSB galaxies are surprisingly abundant, but the surveys were incomplete and a more systematic set of HI observations of a homogeneous sample were required.

To search for additional massive LSB galaxies we undertook a second survey, using a combination of (1) 241 LSB galaxies selected from the online Lyon Extragalactic Database (HyperLeda; <http://leda.univ-lyon1.fr>) on their mean surface brightness in the  $B$  band (referred to as the HyperLeda sample), and (2) 119 LSB galaxies from the UGC (Nilson 1973) with morphological types Sd-m (the UGC sample). Initially the HyperLeda sample was observed in HI using the Arecibo,

Green Bank, and Nançay radio telescopes, while the UGC sample was observed at Nançay only. At a later stage, the Green Bank Telescope (GBT) was used for follow-up HI observations of both samples, to clarify any potential (radio frequency interference (RFI), or other) confusion regarding prior detections and to search for prior nondetections.

The selection of the two samples of LSB galaxies we observed in the 21 cm HI line is described in Section 2, the observations and the data reduction are presented in Section 3, and the results in Section 4. A discussion of the results is given in Sections 5 and 6, and our conclusions are presented in Section 7. The Appendix provides details of many of the individual galaxies observed.

Please note that throughout this paper a Hubble constant value of  $H_0 = 70 \text{ km s}^{-1} \text{ pc}^{-1}$  is used, and that all radial velocities are heliocentric and calculated according to the conventional optical definition  $\left( V = cz = c \left( \frac{\lambda - \lambda_0}{\lambda_0} \right) \right)$ .

## 2. Galaxy Sample Selection

The HyperLeda and UGC galaxy samples were defined in 2004 and 2002, respectively, before the stream of galaxy redshifts from the Sloan Digital Sky Survey (SDSS; see, e.g., York et al. 2000) became available. All values used here reflect the most recently available information, but this results in a few galaxies that are included in the sample which would not have been selected based on the more recently updated spectroscopic velocities and photometric values.

### 2.1. HyperLeda Sample

The HyperLeda galaxies were selected from the HyperLeda database (see, e.g., Makarov et al. 2014), based on the following criteria, as available in 2004:

1. Average blue surface brightness  $\langle \mu_B \rangle \geq 25 \text{ mag arcsec}^{-2}$ , defined following Bothun et al. (1985), to select for galaxies with an LSB disk:  $\langle \mu_B \rangle = B_T + 2.5 \log(D_{25}) + 8.63$ . Here  $B_T$  is the apparent total blue magnitude and  $D_{25}$  the blue major axis diameter in arcminutes, both at the  $25 \text{ mag arcsec}^{-2}$  isophotal level;

**Table 3**  
Results: H I Detections, Values for Individual Telescopes When More Than One Telescope Observed a Galaxy (HyperLeda Sample)

Name	Notes	Conf.	$V_{\text{HI}}$ ( $\text{km s}^{-1}$ )	Error	$W_{50}$ ( $\text{km s}^{-1}$ )	Error	$W_{20}$ ( $\text{km s}^{-1}$ )	Error	rms Jy	Flux ( $\text{Jy km s}^{-1}$ )	Error	$M_{\text{HI}}/M_{\odot}$	Error	Tel.
ESO 368-004	Y	1	1396	1	58	2	78	3	3.78	12.91	0.23	9.04	0.01	N
ESO 368-004	Y	1	1397	1	86	1	101	1	1.50	14.51	0.14	9.09	0.00	G
ESO 368-004	Y	1	1397	5	89	10	108	15	1.30	13.45	0.11	9.06	0.00	G
ESO 424-009	N	1	4057	6	140	12	174	18	3.70	3.27	0.34	9.40	0.05	N
ESO 424-009	N	1	4052	1	153	2	165	3	1.00	3.22	0.13	9.39	0.02	G
ESO 463-005	Y	2	2809	3	519	6	552	9	2.80	11.70	0.46	9.64	0.02	N
ESO 463-005	Y	2	3014	10	159	15	191	15	1.41	3.26	0.17	9.15	0.02	G
ESO 491-003	Y	1	7166	11	154	22	221	34	2.77	2.22	0.26	9.73	0.05	N
ESO 491-003	Y	1	7167	15	202	10	221	10	0.80	1.94	0.11	9.68	0.02	G
ESO 492-001	Y	1	6599	7	124	14	171	21	3.08	3.52	0.28	9.86	0.03	N
ESO 492-001	Y	1	6590	17	208	34	333	54	1.20	4.52	0.22	9.97	0.02	G
ESO 492-001	Y	1	6597	15	206	30	246	46	1.15	3.54	0.16	9.87	0.02	G
...							...							...

(This table is available in machine-readable form.)

- Morphological type later than Sb, to ensure galaxies have a disk and to increase the likelihood of detection in H I;
- Optical diameter  $D_{25} > 30''$ , to ensure against selecting dwarf galaxies;
- No known redshift (at the time of observation, in 2004);
- Inclination  $< 70^\circ$ ;
- Decl.  $-38^\circ < \delta < 80^\circ$  to allow for observation by the radio telescopes.

The complete list of galaxies meeting these criteria comprised  $\sim 290$  objects. Of these, 241 were randomly selected for observation. (The complete sample could not be observed due to limitations in telescope availability.)

### 2.2. UGC Sample

The UGC galaxies were selected from the complete set of UGC dwarf and LSB galaxies that were originally observed by Schneider et al. (1990) and Schneider et al. (1992) in H I, which comprises all listed dwarf, irregular, and Magellanic galaxies in the UGC—a total of 1845 galaxies, or 14% of the total of 12,940 galaxies in the catalog. The original observations were made with the 305 m Arecibo telescope and at the Green Bank 300 foot telescope otherwise. Most of the Green Bank detections were of nearby, H I-rich dwarfs only, due to the telescope's narrow bandpasses ( $3000 \text{ km s}^{-1}$ ) and low sensitivity.

By 1992, 85% were detected and by 2002, when we defined our present sample, the total detection rate had increased to  $> 90\%$ , but more than 180 sources remained undetected. We selected all 119 remaining objects which lie outside the Arecibo declination range for observation at Nançay, excluding the following six objects whose declination is too high ( $> 82^\circ$ ) for the telescope's geometry (see below) to allow tracking: UGC 3461, UGC 5298, UGC 9478, UGC 10263, UGC 10581, and UGC 10605. The nondetections from the Arecibo sample were not reobserved with Nançay, as their nondetection limit is below what is practical with the Nançay. The GBT was later used to confirm a number of the Nançay detections and to look for nondetections from this subsample, as described in Section 3.

## 3. Observations and Data Reduction

### 3.1. The Arecibo Telescope

The Arecibo observations of the HyperLeda sample were carried out between 2004 November 26 and 2005 May 14 for a total of 32 hr of observing time. To avoid baseline ripples caused by the Sun, all the observations were made at night. The position-switching technique was applied, using an on/off pattern with equal time given to the on-source and off-source positions. The on-source integration time was 5 minutes for each galaxy. The backend was configured using nine-level sampling with the Wide band Arecibo Pulsar Processors (WAPPs) and  $5 \text{ km s}^{-1}$  resolution. This allowed for a velocity coverage of either a low velocity range of  $\sim -2000$ – $19,000 \text{ km s}^{-1}$  (1330–1430 MHz), or a high-velocity range of  $\sim 19,000$ – $36,000 \text{ km s}^{-1}$  (1250–1330 MHz) for the two correlator boards separately. It should be noted that large sections of the high-velocity range were filled with RFI and that the rms noise levels in this band listed in the tables were measured in RFI-free sections. The original  $5.3 \text{ km s}^{-1}$  velocity resolution was kept throughout the data processing phase.

The data were calibrated using the on-telescope noise diodes, from the original WAPP files including the two different velocity search ranges. Data analysis was performed using Supermongo routines developed by our team. The two polarizations were first averaged for each observation of a given galaxy, from which the overall rms noise level was measured by choosing a broad range without apparent unusual signatures. Obviously bad data were abandoned at this stage. After that, a polynomial baseline was fitted to the data within the vicinity of the galactic H I profile, excluding those velocity ranges with H I line emission (both from the galaxy and the target galaxy) or RFI (e.g., the GPS L3 signal around  $8300 \text{ km s}^{-1}$ ). With a view toward optimization and faithfulness of the fitting, F-tests were performed on all the orders (0–9) of the polynomial fit and those that gave a result greater than 10 were considerably preferred. Fits of order higher than 4 were rarely adopted, and only the first-order fit was used for profiles with low signal-to-noise ratios (S/Ns). Once the baseline was subtracted, the velocities were corrected to the optical, heliocentric system.

At 21 cm the Arecibo beam is  $3'4 \times 3'6$ .



### 3.2. The Robert C. Byrd GBT

The first observations of the HyperLeda sample galaxies taken with the Robert C. Byrd GBT were taken in 2004 October over a total of nine nights for a total of 65 hr. All these observations used the Gregorian  $L$ -band receiver with the (now retired) auto-correlation spectrometer (Escoffier & Webber 1998). As the redshifts for the observed galaxies were unknown, the spectrometer was set up to observe with a nine-level sampling, from  $-2000$  to  $25,600$   $\text{km s}^{-1}$  (1300–1430 MHz) with  $2.57$   $\text{km s}^{-1}$  resolution, which was smoothed to  $5.2$   $\text{km s}^{-1}$  during the data processing phase. Standard position-switching techniques were used, with an on/off source pattern and 300 s for to each on-source and off-source observation. A calibration noise diode was fired on blank sky at the end of each on+off observing pair.

Follow-up observations of a number of the previously undetected galaxies from the HyperLeda sample were taken with the GBT in early 2012. Again the auto-correlation spectrometer was used for the observations, with the same set-up as for the earlier observations. Position switching was used, with typically 3–5 on-source observations were taken for every off (the total number depending on available telescope time).

A second round of follow-up observations was made in the fall of 2022 to examine discrepancies among our prior detections, between our detections and those from the literature, and to try to detect the previously undetected galaxies from both the UGC and HyperLeda samples. Again the GBT's  $L$ -band receiver was used, but now with the VEGAS spectrometer (Prestage et al. 2015). To maximize coverage, the backend was set up to observe from  $-2000$  to  $30,250$   $\text{km s}^{-1}$  (1290 to 1430 MHz) with  $0.15$   $\text{km s}^{-1}$  velocity resolution, which was smoothed to  $5$   $\text{km s}^{-1}$  during the data processing phase. Please note though, that the presence of RFI at the lower frequencies limited the usable observing range to  $-2000$ – $25,600$   $\text{km s}^{-1}$ , i.e., the same as for the earlier GBT observations. Position switching was again used, with 300 s scans. To maximize our science output from the telescope and take advantage of the very stable baseline on the GBT, the observing pattern consisted of one on+off source pair of scans, typically followed by eight on-source observations, and a final on+off pair. This pattern was used for all observations, if time allowed.

All data were calibrated using the engineering noise diode values measured at the GBT and checked by observing a minimum of one (and typically 2–3) standard flux calibrators each night.

Data were reduced using standard GBTIDL (<http://gbtidl.nrao.edu>) routines modified for our observing pattern. Any individual spectra showing baseline ripples due to RFI were removed from the data reduction package. Frequencies were converted to radial velocities in the optical, heliocentric velocity frame. Data obtained in 2022 were boxcar smoothed to  $5$   $\text{km s}^{-1}$  resolution, to match the  $5.2$   $\text{km s}^{-1}$  resolution for the first sets of observations.

It should be noted that changes in instrumentation between observations make the averaging of the data together impractical.

At 21 cm, the GBT HPBW is  $8.7 \times 8.7$ .

**Table 4**  
H I RMS Values in Millijansky for All Nondetections

Name	Sample	Notes	Nançay	GBT	Arecibo	
					Low	High
ESO 366-014	HL	N	2.61	1.11		
ESO 435-001	HL	N		0.95		
ESO 491-002	HL	Y	1.69			
ESO 527-015	HL	N	3.18			
ESO 540-030	HL	Y	2.58	1.84		
ESO 582-010	HL	N	1.62			
ESO 598-019	HL	N	1.45			
PGC 4620	HL	N	2.08			
PGC 6166	HL	N		0.79	0.52	0.74
PGC 13131	HL	N	3.63	0.98		
PGC 18942	HL	N		0.87		
PGC 21302	HL	N	4.57	0.91		
PGC 21907	HL	N		2.80		
PGC 22928	HL	N		0.88		
PGC 30860	HL	N	3.51			
PGC 39076	HL	N	3.47	1.03	0.23	
PGC 40135	HL	N		1.58	0.35	0.58
PGC 40267	HL	N			0.24	0.35
PGC 52168	HL	N		2.08		
PGC 60361	HL	N		1.08		
PGC 70074	HL	N		1.12		
PGC 75981	HL	N	1.68	1.56		
PGC 77140	HL	N		1.11		
PGC 79534	HL	N	3.61	0.93		
PGC 83540	HL	N		0.93	0.42	
PGC 87255	HL	N		0.87	0.52	0.68
PGC 91383	HL	N			0.18	0.29
PGC 2815827	HL	N	2.66			
UGC 45	UGC	N	4.6			
UGC 190	UGC	N	2.7	0.90		
UGC 239	UGC	N		1.06		
UGC 293	HL	N		1.22	0.36	0.36
UGC 502	HL/UGC	N	2.27	0.54		
UGC 1800	HL	N		0.89	0.56	0.56
UGC 1836	UGC	N	3.3	0.92		
UGC 2314	HL/UGC	N		1.23		
UGC 2436	UGC	N	1.8	1.19		
UGC 2668	HL/UGC	Y	2.96	2.86		
UGC 2724	UGC	N		2.30		
UGC 3041	HL	Y	1.64	0.81		
UGC 3566	UGC	N	2.5			
UGC 3814	UGC	N	2.9			
UGC 3963	UGC	Y		1.93		
UGC 4194	UGC	N	6.3	1.04		
UGC 5071	UGC	Y	3.3/10.7	1.82		
UGC 5613	UGC	Y	...			
UGC 6812	UGC	Y	3	0.98		
UGC 7110	UGC	N	4.6	0.96		
UGC 8176	UGC	N	3.4			
UGC 10704	HL	N		0.92		
UGC 11207	HL	N	1.83	1.09		

(This table is available in machine-readable form.)

### 3.3. The Nançay Radio Telescope

The 100 m class Nançay decimetric Radio Telescope (NRT), a meridian transit-type instrument of the Kraus/Ohio State design, consists of a fixed spherical mirror (300 m long and 35 m high), a tiltable flat mirror (200×40 m), and a focal

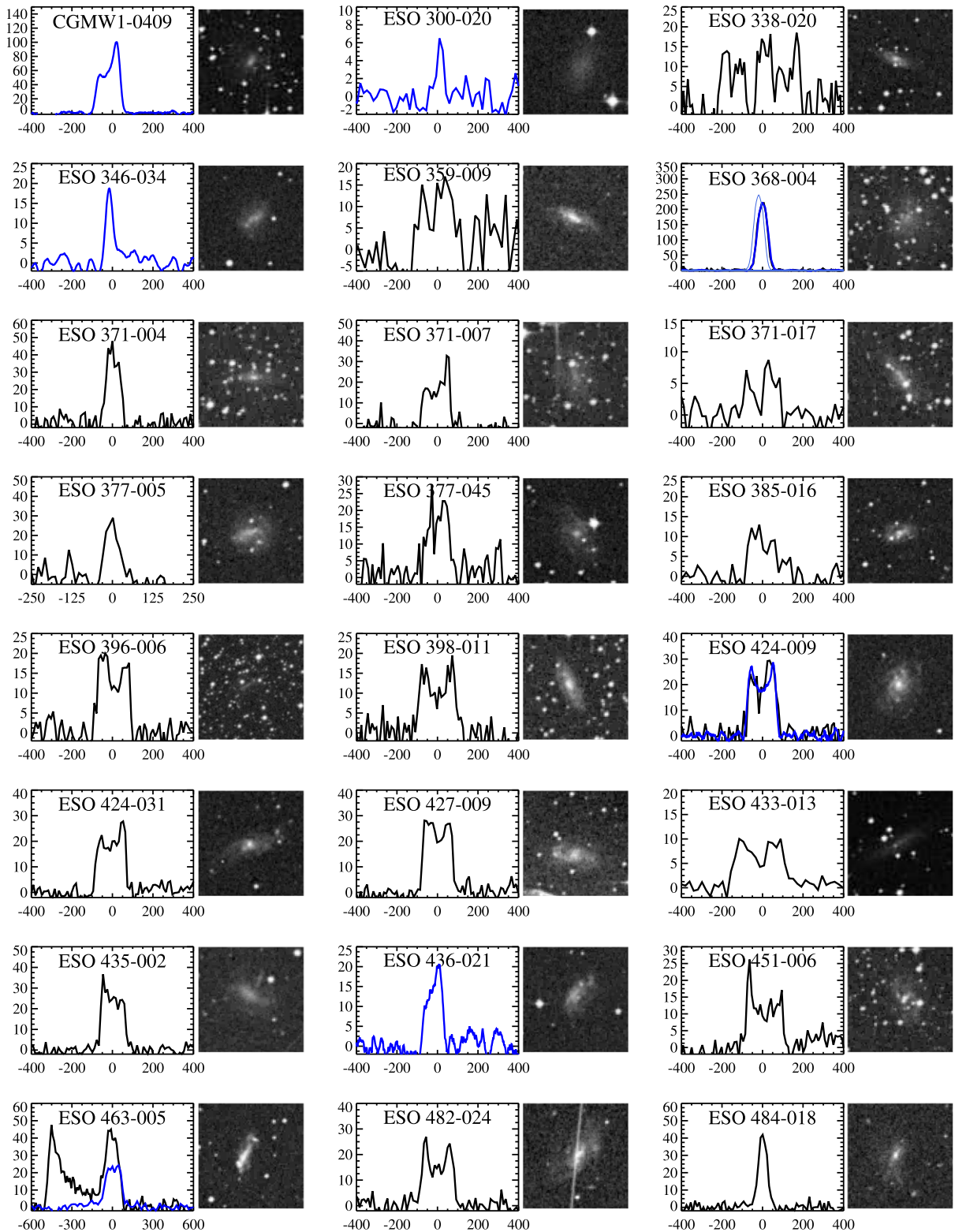


**Figure 1.** 21 cm H I line spectra and optical images of the detected galaxies. Black lines in the spectra represent Nançay data, blue lines GBT data, and red lines Arecibo data. In the case where an object was observed twice by the same telescope, the earliest observation is shown by a dashed line. Optical images are  $2 \times 2$  arcmin in size. False color (*i*, *r*, and *g* filter) images are from SDSS DR12 (Alam et al. 2015), and black and white images are from the 2nd Digitized Sky Survey (DSS2) blue plates (Abazajian et al. 2004), used when SDSS images are not available. Objects are arranged in alphabetical order. The complete figure set (13 images) is available in the online journal.

carriage moving along a curved rail track; for further details on the instrument and data reduction, see van Driel et al. (2016) and references therein. Sources on the celestial equator can be

tracked for about 60 minutes. Its collecting area is about  $7000 \text{ m}^2$  (equivalent to a 94 m diameter parabolic dish). Due to the east–west elongated shape of the mirrors, some of the

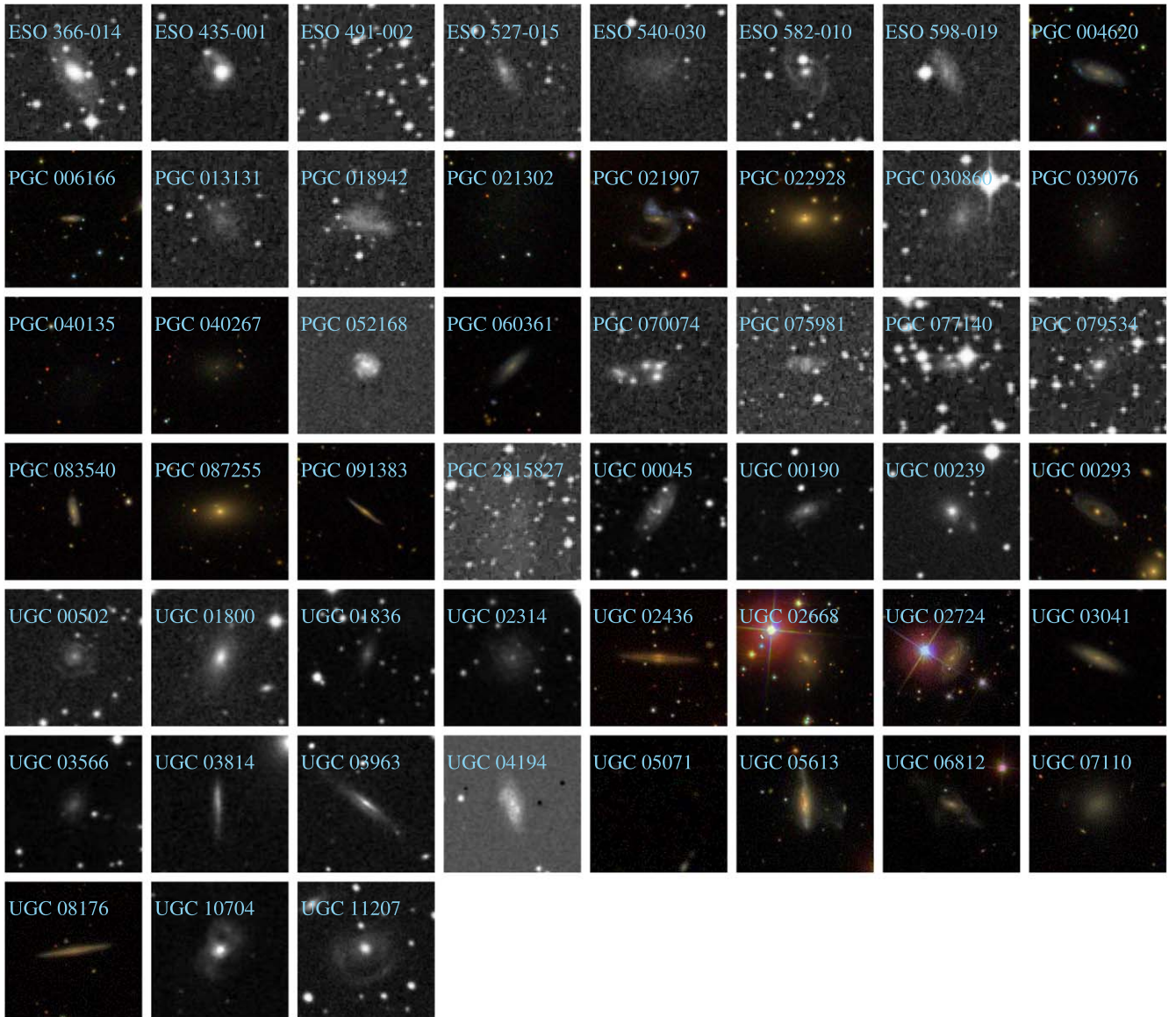


**Figure 2.** Optical images of target galaxies that were not detected by us in H I. Images are  $2 \times 2$  arcmin in size, unless otherwise indicated in the lower right corner. False color (*i*, *r*, and *g* filter) images are from SDSS DR16 (Ahumada et al. 2020) and black and white images are from DSS2 blue plates (Abazajian et al. 2004), used when DR16 images are not available. Objects are arranged in alphabetical order.

instrument’s characteristics depend on the observed declination. At 21 cm, the telescope’s half-power beam width (HPBW) is  $3/5$  in R.A., independent of declination, while in the north–south direction it is  $23'$  for declinations up to  $\sim 20^\circ$ , rising to  $25'$  at  $\delta = 50^\circ$  and  $38'$  at  $\delta = 79^\circ$ , the northern limit of the survey. The instrument’s effective collecting area and, consequently, its gain, follow the same geometric effect, decreasing correspondingly with declination. Flux calibration is determined through regular measurements of a cold load calibrator and periodic monitoring of strong continuum sources.

All data were taken in a standard on/off position-switching mode, with an on-source integration time step of 40 s. An autocorrelator set-up of 4096 channels was used in a 50 MHz bandpass, with a velocity resolution of  $2.6 \text{ km s}^{-1}$ . For most of the HyperLeda objects the default search range was  $\sim -250$ – $10,600 \text{ km s}^{-1}$ , whereas for the UGC sample it was  $\sim 325$ – $11,825 \text{ km s}^{-1}$ . For a number of objects with known higher redshifts, a search was also made at  $\sim 6875$  to  $18,330 \text{ km s}^{-1}$  (for four objects

from the HyperLeda sample and 25 from the UGC sample). The bulk of the observations of the HyperLeda sample galaxies were made in the period 2004 July–November, for a total of about 410 hr of telescope time, and the high-velocity observations were obtained in 2007, whereas the UGC sample observations were made in the period 2003 January–December, using a total of about 240 hr of telescope time.

Averaging the two receiver polarizations and applying a declination-dependent factor to convert from units of system temperature to flux density in Jansky was done using standard NRT software. In order to reduce the effect of relatively strong RFI in our observations, we used the RFI flagging and mitigation routine described in Monnier Ragaigine et al. (2003a). The RFI signal trigger was usually set to a level of  $10\sigma$  for each 40 s integration. Subsequent smoothing in velocity and baseline fitting was performed for the HyperLeda sample with standard Nançay software and for the UGC sample with Supermongo routines developed by one of our team,



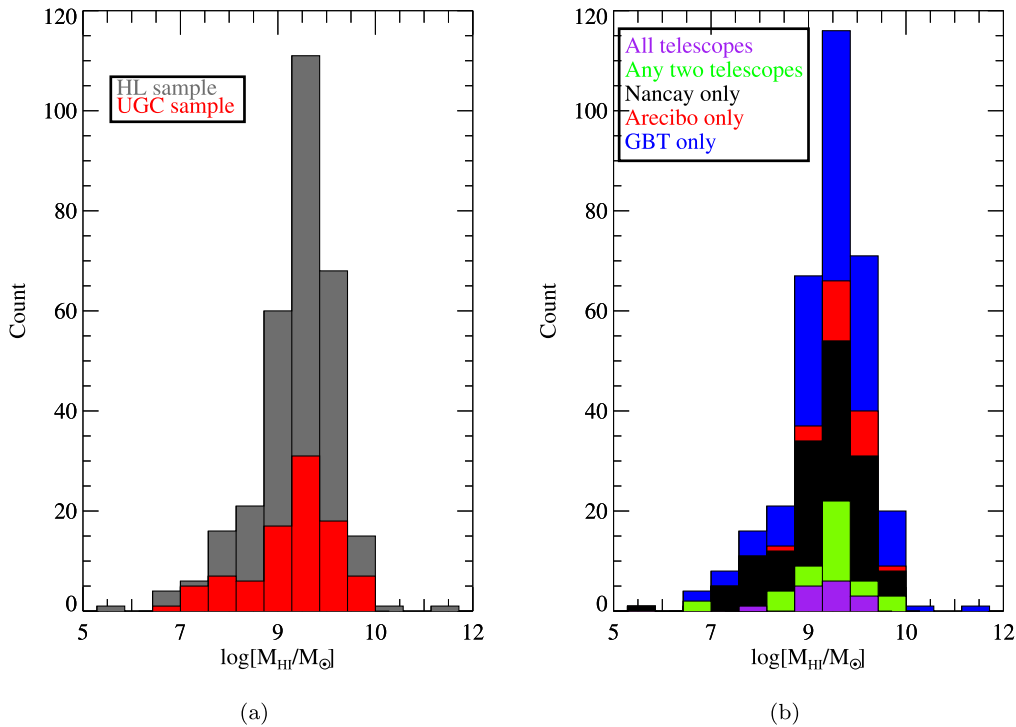


**Figure 3.** Distributions of the total H I mass  $M_{\text{HI}}$ , in solar masses, for all detected galaxies in our survey: (a) comparison between the UGC sample (red) and the HyperLeda sample (gray), and (b) as a function of the telescope(s) which detected the galaxy.

which were based on the standard ANALYZ routines then in use at Arecibo.

Spectra with an H I line peak S/N larger than 5 were boxcar smoothed to a velocity resolution of  $10 \text{ km s}^{-1}$  during the data reduction, whereas spectra with fainter lines and nondetections were smoothed to a resolution of  $18 \text{ km s}^{-1}$ . Radial velocities were ultimately converted to a heliocentric, optical  $cz$  scale.

## 4. Results

### 4.1. Literature Properties

Basic optical properties, including spectroscopic radial velocities, of the sample galaxies are listed for both H I detections and nondetections in Table 1. Details on the individual galaxies, when given, can be found in the Appendix. From the optical parameters (see the list hereafter), the total blue magnitude,  $B_T$ , and the axial ratio,  $b/a$ , were taken from HyperLeda.

At present, redshifts are available for 177 of the observed galaxies, with 135 objects having optical spectroscopic redshifts (only), 80 having previously published H I redshifts, and 38 having both optical and H I redshifts in the literature (see Tables 1 and 4). References for all redshifts found are given in Table 1, and are divided into two categories—optical spectral line and H I velocities.

Listed in Table 1 are the following elements, in alphabetical order of galaxy name, and divided into four categories: galaxies detected in H I, spurious detections, galaxies not detected in H I, and galaxies whose optical velocity measurements (taken after our observations) place them outside the H I search range. Please note that we have listed the current HyperLeda values in our tables and used them for calculations.

1. Name: common name of the object;
2. R.A.: right ascension in J2000.0 coordinates;

3. Decl.: decl. in J2000.0 coordinates;
4. Type: morphological type, preferably from the HyperLeda database. If not available, the classification retrieved from the NASA/IPAC Extragalactic Database (NED) <https://ned.ipac.caltech.edu>, is given in brackets;
5.  $B_T$ : total apparent magnitude in the  $B$  band, from HyperLeda;
6.  $D_{25}$ : length of the projected major axis of the galaxy at the isophotal level  $25 \text{ mag arcsec}^{-2}$  in the  $B$  band, from HyperLeda;
7.  $b/a$ : axial ratio measured at a surface brightness level of  $25 \text{ mag arcsec}^{-2}$  in the  $B$  band, from HyperLeda;
8.  $V_{\text{opt}}$ : heliocentric velocity, from optical spectra;
9. Opt. ref.: literature reference for  $V_{\text{opt}}$  (the full references to the abbreviated notations used in the table are given in the notes to the table);
10.  $V_{\text{opt}}$ : heliocentric velocity, from H I spectra;
11. H I ref.: literature reference for  $V_{\text{HI}}$ .

### 4.2. The H I Data

The primary results from the observations are given in Tables 2, 3, and 4. H I spectra and optical images of the detections are shown in Figure 1 and optical images of the nondetections are shown in Figure 2. The H I mass distributions for the samples can be seen in Figure 3.

Tables 2 and 3 give the measured H I line properties of all detected galaxies. Table 2 provides the median and therefore highest-quality values, while Table 3 provides the values as measured by each telescope, for all galaxies which were observed by more than one telescope.

Finally, Table 4 lists the rms noise level values of all nondetections for each telescope.



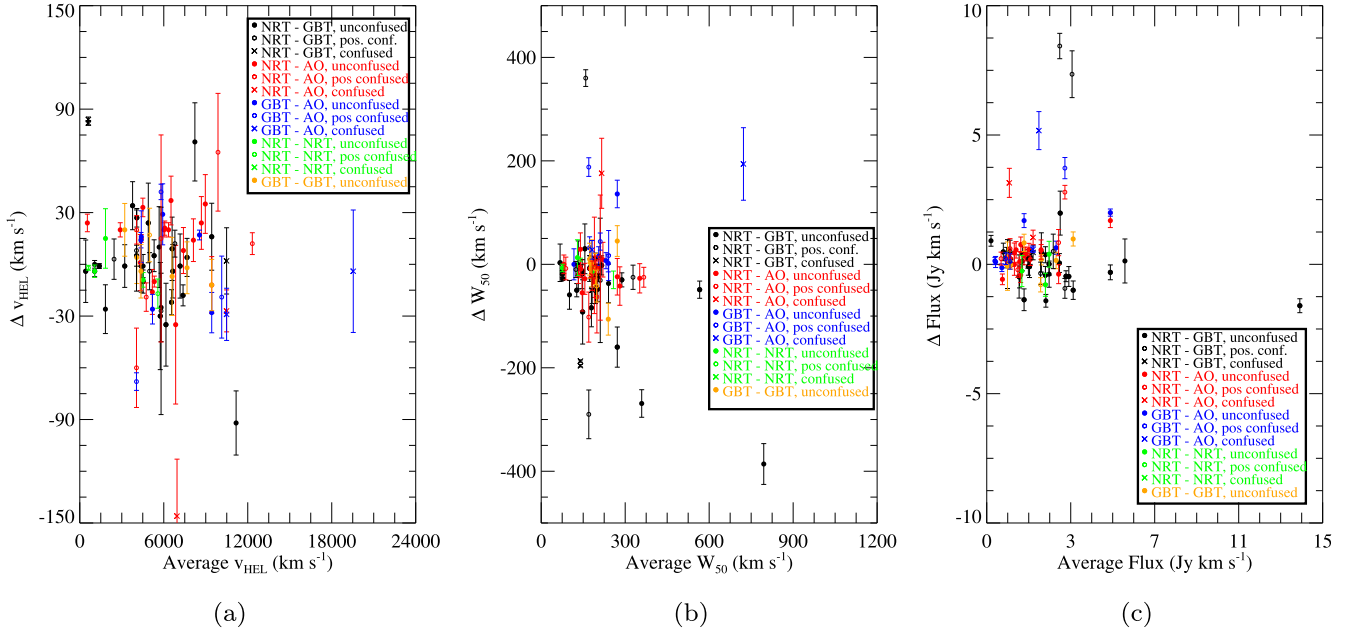


**Figure 4.** Comparison of differences in the H I line profile parameters of the galaxies in our two samples that were detected by us with more than one telescope. Plotted as a function of their average central H I velocity,  $V_{\text{H I}}$ , are the differences in (a) central H I velocity,  $\Delta V_{\text{H I}}$  in kilometers per second, (b) in  $W_{50}$  line width,  $\Delta W_{50}$  in kilometers per second, and (c) in integrated H I line flux,  $\Delta F_{\text{H I}}$  in Jansky kilometers per second. As indicated in the legend, colors indicate which telescopes' results are compared: Green Bank (GBT) vs. Nançay (NRT) in black, Arecibo (AO) vs. NRT in blue, AO vs. GBT in red, and NRT (HyperLeda sample) vs. NRT (UGC sample) in green. Different symbols indicate the probability of a detection being confused by another galaxy within a telescope beam: large filled dots for uncontaminated, crosses for possibly contaminated, and small open dots for clearly contaminated. Outliers in all plots are described in Section 4.3 and the Appendix.

In Table 2, if an object was observed with more than one telescope within the HyperLeda survey, nonweighted averages were used for the measured values, unless one or more of the individual measurements showed a significant discrepancy with the others, such as a much larger estimated uncertainty, lower line flux, or difference in central velocity, in which case they were not used here (see also the notes on individual galaxies in the Appendix).

Listed in Tables 2 and 3 are the following elements for all detected galaxies, in alphabetical order of their name:

1. Name: the common name of the object;
2. Sample: the survey(s) for which the observation was made. The options are: HyperLeda (HL), UGC (UGC), both HyperLeda and UGC (HL/UGC), HyperLeda spurious detection (HLS), and UGC spurious detection (UGCS). Please note that this column only appears in Table 2;
3. Notes: indication if the galaxy has notes in the Appendix; given as Y/N for Yes/No;
4. Conf: contamination (confusion) status for detections, indicating the level of possibility that another galaxy within the telescope beam contributed some or all of the detected H I flux, graded as 1 (unlikely), 2 (possible), and 3 (very likely). For details on the assessment of the contamination status, see the description of potentially confusing sources given in the Appendix for all galaxies with a confusion status of 3 or 2;

(a) For the HyperLeda sample, a search was made (using HyperLeda and NED) within, respectively, a  $12'$  radius and  $1000 \text{ km s}^{-1}$  around the position and systemic velocity of the detected galaxy. If no known source was found within that region, the confusion flag was set to 1, indicating the detection is likely not confused. If a known galaxy lay within that region but

was unlikely to be contributing to the detected H I flux (e.g., the known galaxy is of type S0 or earlier), the confusion status flag was set to 2. If at least one galaxy lay within the region and was very likely to contribute to some or all of the detected H I gas, the confusion status was set to 3.

(b) For the UGC sample, we first inspected DSS images centered on the position of each clearly or marginally detected source, over an area of  $12' \times 36'$  ( $\alpha \times \delta$ ). In case galaxies were noted that might give rise to confusion with the H I profile of the target galaxy, we then queried the NED and HyperLeda databases for information on the objects.

All galaxies with possible contamination have notes in Appendix;

5.  $V_{\text{H I}}$ : central H I line (optical, heliocentric) velocity as measured in our profiles, in kilometers per second;
6. Error: error for  $V_{\text{H I}}$ , determined following Schneider et al. (1986, 1990), as

$$\sigma_{V_{\text{H I}}} = 1.5(W_{20} - W_{50})(S/N)^{-1} \text{ (km s}^{-1}\text{)}, \quad (1)$$

where  $S$  is the peak S/N of the spectrum, which we define as the ratio of the peak flux density  $S_{\text{max}}$  and the rms dispersion in the baseline (both in Jy);

7.  $W_{50}$ : H I line velocity width measured at 50% of the H I profile peak value, in kilometers per second;
8. Error: error for  $W_{50}$ , in kilometers per second (Table 3 only.). For the GBT and Nançay data, these errors are expected to be 2 times those in  $V_{\text{H I}}$ , following Schneider et al. (1990). For the Arecibo data, an upper limit of  $15 \text{ km s}^{-1}$  is given for the errors, i.e., the width of one (smoothed) velocity channel.
9.  $W_{50, \text{cor}}$ : H I line velocity width measured at 50% of the H I profile peak value, in kilometers per second, corrected

**Table 5**  
Galaxies with Large Differences between H I Properties Measured by More Than One Telescope

Object	Confusion (1–3)	$\Delta V_{\text{hel}}$ (km s <sup>-1</sup> )	$\Delta W_{50}$ (km s <sup>-1</sup> )	$\Delta F_{\text{HI}}$ (Jy km s <sup>-1</sup> )	Telescopes	Notes
ESO 463-005	2	<b>-205</b>	<b>360</b>	<b>8.44</b>	Nançay – GBT	Nançay obs. confused
ESO 492-001	1	9, 2	<b>-84, -82</b>	-1.0, 0.0	Nançay – GBT, Nançay – GBT <sub>2</sub>	Nançay obs. low S/N
IC 3852	1	14, 18	<b>3, 108</b>	<b>0.6, 0.5</b>	GBT – AO, GBT <sub>2</sub> – AO	
PGC 16370	1	<b>-198</b>	-49	2.0	Nançay – GBT <sub>2</sub>	Nançay obs. low S/N
PGC 17124	2	3	-25	<b>7.4</b>	Nançay – GBT <sub>2</sub>	Nançay obs. confused
PGC 21133	1	-30	<b>-92</b>	-0.5	Nançay – GBT	Nançay obs have high error
PGC 21529	2	8, <b>-60, -68</b>	<b>-290, -102, 188</b>	-0.9, <b>2.8, 3.7</b>	Nançay – GBT, Nançay – AO, GBT – AO	Nançay & GBT obs. confused
PGC 27849	1	16, 4, -12	<b>-160, -115, -24</b>	<b>-1.4, 0.2, -0.5</b>	Nançay – GBT <sub>2</sub> , Nançay – GBT, Nançay – AO	Nançay obs. confused
PGC 38333	3	<b>-146</b>	<b>176</b>	<b>3.2</b>	Nançay – AO	Nançay obs. confused
PGC 56738	2	<b>65</b>	<b>-63</b>	0.2	Nançay – AO	Nançay obs. confused
UGC 605	3	-4	<b>194</b>	<b>5.17</b>	GBT – AO	GBT obs. confused
UGC 5983	3	<b>82, 84</b>	<b>-187, 196</b>	<b>-46, -44</b>	Nançay – GBT, Nançay – GBT	All obs. confused
UGC 8107	1	<b>71</b>	<b>-386</b>	0.1	Nançay – GBT	

**Note.** Bold values match the values listed under the column Telescopes.

for random motion effects, using Tully & Fouque (1985), and inclination

$$W_{50,\text{cor}} = \sqrt{W_{50,i}^2 + W_r^2 + 2W_{50,i}W_r[1 - e^{-(W_{50,i}/W_r)^2}] - 2W_r^2e^{-(W_{50,i}/W_r)^2}}. \quad (2)$$

Here,  $w_r$  is the assumed turbulent motion, which is 14 km s<sup>-1</sup> for LSB galaxies (O'Neil et al. 2000) and  $W_{50,i} = W_{50}/[\sin(i)]$ , where the inclination is based on the  $b/a$  axial ratio listed in Table 1.

10.  $W_{20}$ : H I line velocity width measured at 20% of the H I profile peak value, in kilometers per second;
11. Error: error for  $W_{20}$ , in km s<sup>-1</sup>. For the GBT and Nançay data, these errors are expected to be 3.1 times those in  $V_{\text{HI}}$ , following Schneider et al. (1990). For the Arecibo data, the listed errors are 15 km s<sup>-1</sup> (see  $W_{50}$  error). (Table 3 only.)
12. rms: rms noise level of the H I spectrum, in millijansky, measured around the detected H I line. For Table 2 if the detection was made with more than one telescope only the rms for the most sensitive observation is given;
13.  $F_{\text{HI}}$ : measured integrated H I line flux, in jansky kilometers per second;
14. Error: error for  $F_{\text{HI}}$ , in jansky kilometers per second, determined following Schneider et al. (1986, 1990), as

$$\sigma_{F_{\text{HI}}} = 2(1.2W_{20}R)^{0.5}\text{rms}(\text{km s}^{-1}), \quad (3)$$

where  $R$  is the instrumental resolution in kilometers per second (see Section 3);

15.  $M_{\text{HI}}$ : log of the total H I mass in units of solar mass, where  $M_{\text{HI}} = 2.356 \times 10^5 D^2 F_{\text{HI}}$ , and  $D = V/70$  is the galaxy's distance (in megaparsecs);
16. Error: error for  $\log(M_{\text{HI}}/M_{\odot})$ ;
17. Telescope: telescope(s) used for observation:  $A$  = Arecibo,  $G$  = GBT, and  $N$  = Nançay. The number of times a telescope is listed denotes the number of separate observations made with that telescope over the duration of our survey.

Listed in Table 4 are the following elements for all galaxies not detected by any telescope, in alphabetical order of their name.

1. Name: the common name of the object;

2. Sample: which survey resulted in this detection. The options are: HyperLeda (HL), UGC (UGC), and both (HL/UGC);
3. Notes: indicating if a galaxy has notes in Appendix (see Table 2 for a description);
4. Nançay: rms noise level across the observed spectra, in mJy, for all Nançay observations. For the HyperLeda sample, the search range is  $-250$ – $10,600$  km s<sup>-1</sup>. For the UGC sample a single value indicates a search was made only in the “lo” range,  $325$ – $11,825$  km s<sup>-1</sup>, and a second value an additional search in the “hi” range,  $\sim 6875$ – $18,330$  km s<sup>-1</sup>;
5. GBT: rms noise level across the observed spectra, in millijansky, for all GBT observations, in the range  $2000$ – $25,600$  km s<sup>-1</sup>;
6. Arecibo low: rms noise level across the observed spectra, in millijansky, for all Arecibo observations in the low velocity range,  $-2000$ – $19,000$  km s<sup>-1</sup>;
7. Arecibo high: rms noise level across the observed spectra, in millijansky, for all Arecibo observations in the high-velocity range,  $19,000$ – $36,000$  km s<sup>-1</sup>.

### 4.3. Intertelelescope Comparisons

#### 4.3.1. Telescope–Telescope Comparison

Of the 350 galaxies observed for this paper, the majority (255, or 72.9%) was observed with only one telescope. The remaining 95 galaxies, though, allow for a comparison of H I profiles detected with the different instruments. Included within these statistics are the 14 galaxies detected in both the UGC and HyperLeda surveys.

In all, then, the breakdown between the samples is:

1. Sixty-three galaxies observed by both the GBT and Nançay telescopes (eight were observed twice by the GBT);
2. Twenty galaxies observed by both the Arecibo and Nançay telescopes;
3. Six galaxies observed by both the Arecibo and GBT telescopes;
4. One galaxy observed only at Nançay but separately for the UGC and HyperLeda samples;

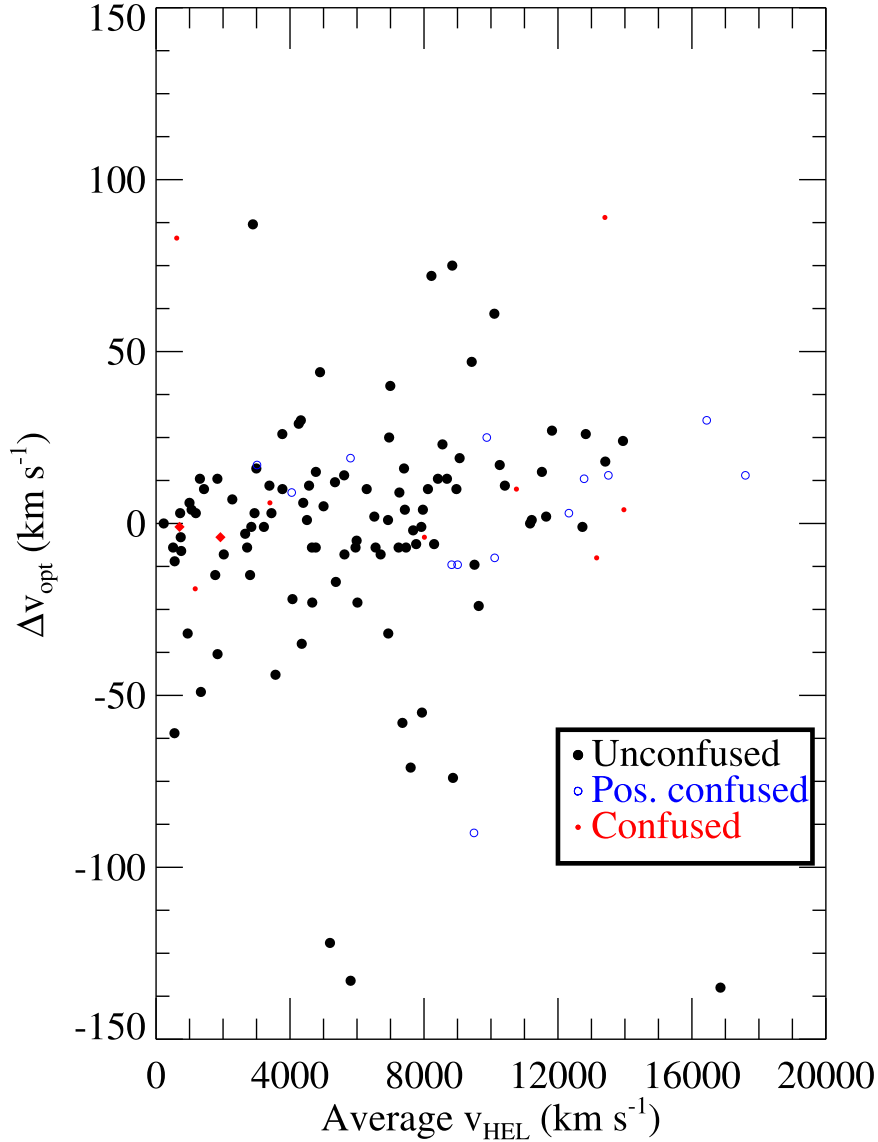


**Figure 5.** Differences between our central H I line velocities and averaged values of the optical velocities listed in the literature,  $\Delta v_{\text{opt}}$  in kilometers per second, as a function of optical velocities from the literature,  $V_{\text{hel}}$  kilometers per second, for the galaxies in our combined sample. As indicated in the legend, colors indicate the probability of a detection being confused by another galaxy within the telescope beam: black for uncontaminated, blue for possibly contaminated, and red for likely contaminated.

5. Five galaxies observed by all three telescopes.

These intertelescope comparisons are shown in Figure 4 for H I profile central velocities,  $W_{50}$  velocity widths, and integrated line fluxes. Overall, they are consistent.

Comparison between the central velocities measured by the different telescopes/surveys shows a spread of differences centered around  $1 \pm 4 \text{ km s}^{-1}$  for the 54 galaxies not contaminated by a nearby companion and observed by more than one telescope (indicated by filled dots in Figure 4). The comparisons between the individual telescope are consistent, with the Nançay and GBT telescopes having the smallest differences, but small number statistics makes drawing any conclusions difficult. The differences between the telescopes and their standard errors are  $v_{\text{NRT}} - v_{\text{GBT}} = -1 \pm 8 \text{ km s}^{-1}$ ;  $v_{\text{GBT}} - v_{\text{AO}} = 16 \pm 9 \text{ km s}^{-1}$ ;  $v_{\text{NRT}} - v_{\text{AO}} = 18 \pm 4 \text{ km s}^{-1}$ ;  $v_{\text{NRT,UGC}} - v_{\text{NRT,HL}} = -2 \pm 4 \text{ km s}^{-1}$ ; and  $v_{\text{GBT}} - v_{\text{GBT}} = 0 \pm 3 \text{ km s}^{-1}$ .

The  $W_{50}$  profile widths measured for uncontaminated detections are also similar. The measured  $W_{50}$  values for the 54

**Table 6**  
Galaxies with  $|V_{\text{H I}} - V_{\text{opt}}| > 100 \text{ km s}^{-1}$

Object $v$	$V_{\text{H I}}$ ( $\text{km s}^{-1}$ )	$V_{\text{opt}}$ ( $\text{km s}^{-1}$ )	Note
PGC 7225	5193	$5071 \pm 80$	1
UGC 263	16,853	$16,718 \pm 105$	2
UGC 1145	5809	$5676 \pm 13$	3

**Note.** (1) Our H I results are confirmed by two telescopes—see the Appendix. (2)  $V_{\text{opt}}$  has a  $\pm 100 \text{ km s}^{-1}$  error, putting it close to our measured value. (3) Peak  $V_{\text{H I}}$  value confirmed by two telescopes—see the Appendix.

uncontaminated galaxies averaged  $\Delta W_{50} = -8 \pm 9 \text{ km s}^{-1}$ . Here the NRT and Arecibo values are the most similar. The differences between the telescopes and their standard errors are  $W_{50,\text{NRT}} - W_{50,\text{GBT}} = -19 \pm 16 \text{ km s}^{-1}$ ;  $W_{50,\text{GBT}} - W_{50,\text{AO}} = 16 \pm 21 \text{ km s}^{-1}$ ;  $W_{50,\text{NRT}} - W_{50,\text{AO}} = -9 \pm 9 \text{ km s}^{-1}$ ;  $W_{50,\text{NRT,UGC}} - W_{50,\text{NRT,HL}} = 7 \pm 14 \text{ km s}^{-1}$ ; and  $W_{50,\text{GBT}} - W_{50,\text{GBT}} = 2 \pm 15 \text{ km s}^{-1}$ .

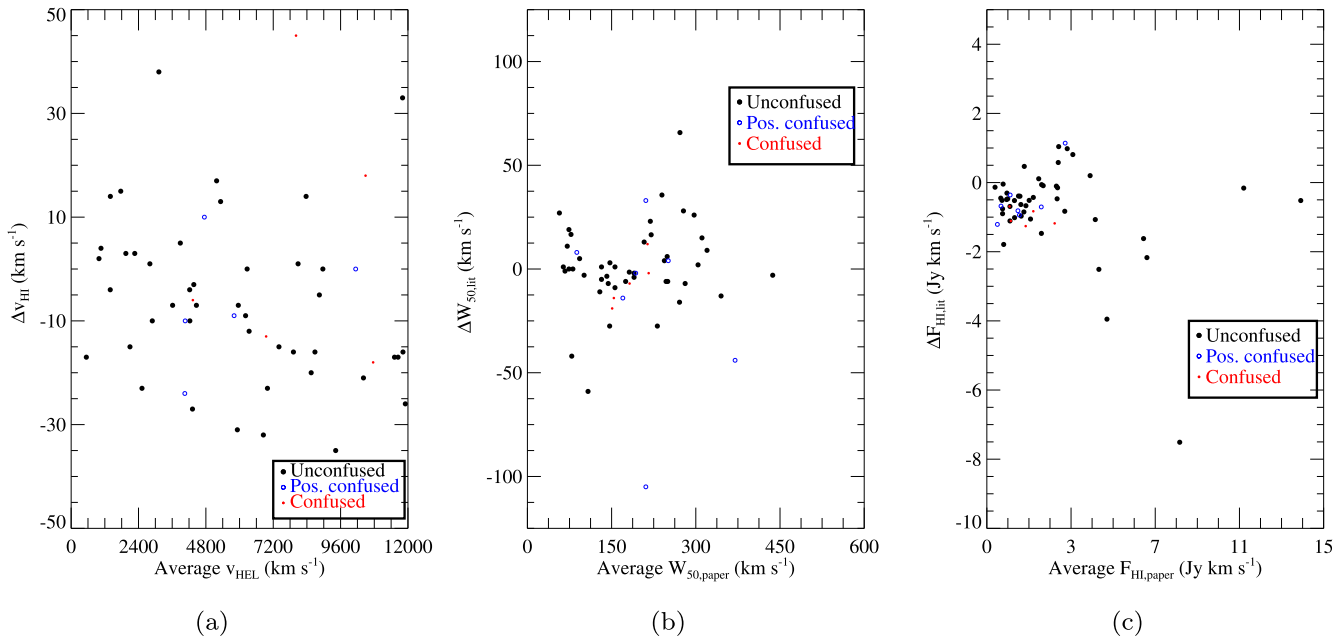


**Figure 6.** Comparison of differences in average H I line profile parameters as measured by us with averages of values listed in the literature, for the galaxies in our combined sample. Plotted as a function of our average H I line parameters are the differences in: (a) central velocity,  $\Delta V_{\text{H I}}$  in kilometers per second, (b)  $\Delta W_{50}$  line width, in kilometers per second, and (c) integrated line flux,  $\Delta F_{\text{H I}}$  in Jansky kilometers per second. As indicated in the legend, colors indicate the probability of a detection being confused by another galaxy within the telescope beam: black for uncontaminated, blue for possibly contaminated, and red for likely contaminated. Please note that panel (a) does not include PGC 38958 (see the [Appendix](#) for an explanation).

The integrated H I line fluxes are comparable as well. Listed here are the differences in the measured flux values for the uncontaminated galaxies, given as a percentage of the galaxies’ flux. Here, the GBT values readily agree with those of Nançay, but the Arecibo values do not agree as well with either telescope. The differences between the telescopes and their standard errors are  $f_{\text{NRT}} - f_{\text{GBT}} = 0.01 \pm 0.08\%$ ;  $f_{\text{GBT}} - f_{\text{AO}} = 0.36 \pm 0.15\%$ ;  $f_{\text{NRT}} - f_{\text{AO}} = 0.22 \pm 0.07\%$ ;  $f_{\text{NRT,UGC}} - f_{\text{NRT,HL}} = 0.04 \pm 0.07\%$ ; and  $f_{\text{GBT}} - f_{\text{AO}} = 0.08 \pm 0.07\%$ . Also in this case, the differences are small compared to the noise for small number statistics.

#### 4.3.2. The Outliers

Table 5 lists all galaxies which were observed by more than one telescope and which show differences in one or more measured H I property that lie outside the ranges listed above. Each of these galaxies is also described in detail in the [Appendix](#).

### 4.4. Comparisons with the Literature

#### 4.4.1. Optical Velocity Comparison

Of the 350 galaxies observed, 177 have previously published spectral line velocities, with 135 having optical (spectroscopic) velocities in the literature. Of these 135, 124 were detected in our survey, and of these 101 are unlikely to be confused with any other object within the telescope beam.

Figure 5 shows the difference between our  $V_{\text{H I}}$  central H I velocities (see Table 2) and the optical spectroscopic velocities (hereafter referred to as “optical velocities”) found in the literature, as a function of  $V_{\text{H I}}$ . Almost all optical velocities are within  $\pm 100 \text{ km s}^{-1}$  of our H I measurements, with a median velocity difference of  $-2 \pm 2 \text{ km s}^{-1}$ . Those galaxies with

velocity differences  $> \pm 100 \text{ km s}^{-1}$  are discussed in Table 6 and the [Appendix](#).

The H I velocities of the three galaxies listed in Table 6 are all likely to be accurate and reliable values. None of their H I profiles are likely to be confused with H I from another galaxy within the beam. Two of the galaxies, UGC 263 and PGC 7225, have rather uncertain optical velocities, which are both only  $< 1.5\sigma$  different from our H I values, and the peak H I velocity of UGC 1145 was confirmed by two telescopes.

#### 4.4.2. H I Literature Values

Published H I measurements are now available for 80 of our detected galaxies. Of these, 66 are of uncontaminated detections. A comparison between the literature values and our measurements is shown in Figure 6 for  $V_{\text{H I}}$ ,  $W_{50}$ , and  $F_{\text{H I}}$ . On average the values match extremely well, with  $\Delta V_{\text{hel}} = -7 \pm 2$ ,  $\Delta W_{50} = 0 \pm 3$ , and  $\Delta F_{\text{H I}} = -0.4 \pm 0.1 \text{ Jy km s}^{-1}$ .

Only one galaxy, PGC 2815809, has significant differences between our measured H I values and those found in the literature, but this may be due to nearby H I source HIPASS J0756-26. Further observations are required to determine if PGC 2815809 and HIPASS J0756-26 are in fact the same object and, if so, where its center lies (see the [Appendix](#) for further details).

## 5. The H I Properties of the Sample

### 5.1. Sample Properties

Figure 7 shows the total H I masses of our 295 detected galaxies as a function of radial velocity ( $V_{\text{H I}}$ ). The plot shows the expected increase of  $M_{\text{H I}}$  with velocity, with most of the lower-mass detections at a given velocity obtained with the much larger Arecibo telescope.



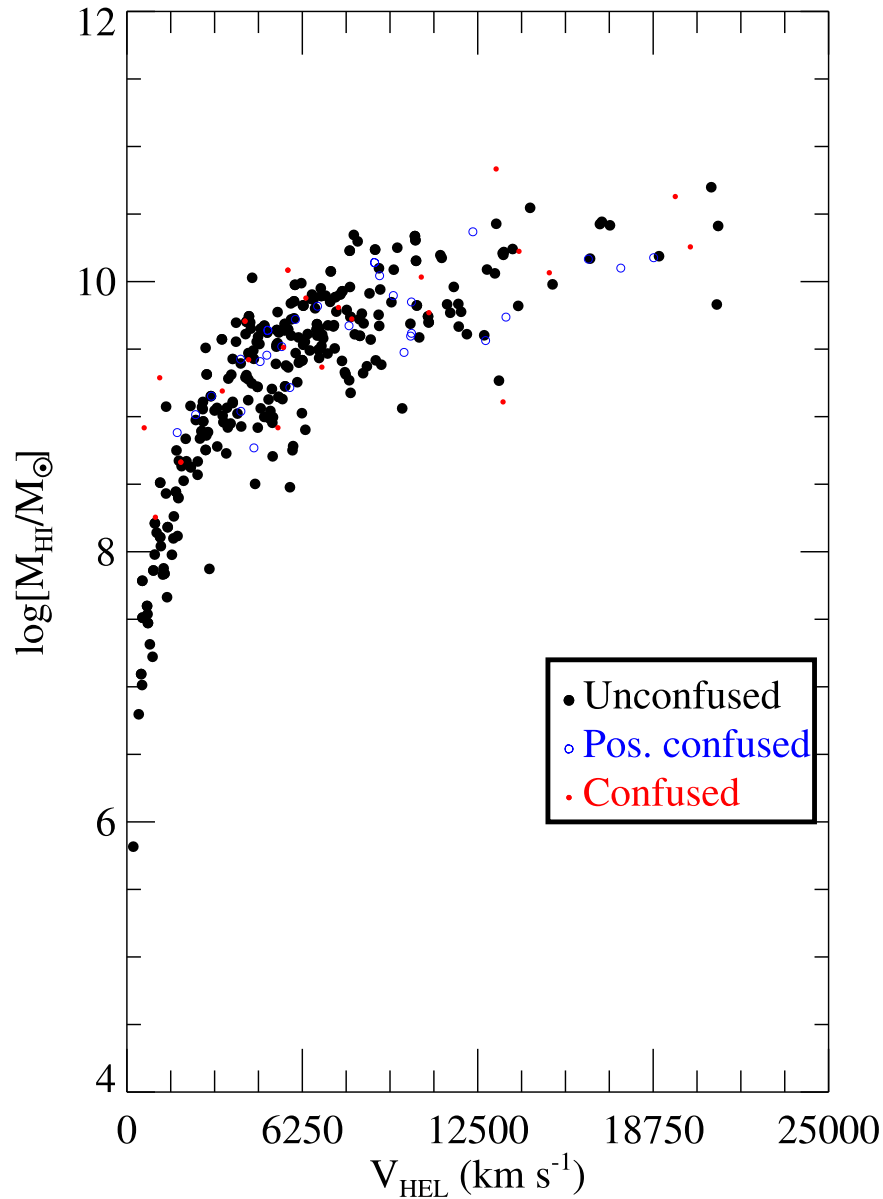


**Figure 7.** Total H I mass,  $\log(M_{\text{HI}})$  in solar masses, as a function of radial velocity,  $V_{\text{hel}}$  in kilometers per second, for the detected galaxies in our combined sample. As indicated in the legend, symbols indicate the probability of a detection being confused by another galaxy within the telescope beam: solid for uncontaminated, open for possibly contaminated, and small for likely contaminated.

Plotted in Figure 8 is the total H I mass as a function of the inclination-corrected  $W_{50,\text{cor}}$  line width, a parameter indicative of the total galaxy mass, again showing the expected increase with  $W_{50,\text{cor}}$  and H I mass.

Looking at the data from this survey, there is no trend between average blue surface brightness  $\langle\mu_{\text{B}}\rangle$  and either H I mass, H I mass-to-luminosity ratio, blue luminosity  $L_{\text{B}}$ , or total mass as indicated by  $W_{50,\text{cor}}$  (see Figures 9 and 10). That is, we do not see any trend toward galaxies becoming less (or more) massive, gas rich, or luminous as their surface brightness decreases. There is, however, a small trend for the upper limit to the  $M_{\text{HI}}/L_{\text{B}}$  ratio to increase as the surface brightness decreases, which is consistent with the idea that the average LSB galaxy is more gas rich than its HSB counterpart, for a given luminosity.

## 5.2. Comparison with the HIPASS 1000 Brightest Galaxies Sample

It is an interesting idea to compare the H I mass distribution of the galaxies in this survey with those found in other H I surveys. It is difficult to find an identical sample, however, as this survey has intentionally avoided selecting galaxies which are likely of low H I mass and catalogs such as Huang et al. (2014) and Lutz et al. (2017) do not contain enough galaxies for a meaningful statistical comparison. The best comparison sample is likely the HIPASS 1000 H I Brightest Galaxy Catalog (BGC; Koribalski et al. 2004). Figure 11 shows a comparison of the cumulative distribution of the H I masses of the three galaxy samples (BGC, and our HyperLeda and UGC), and it is clear that the samples appear similar, but certainly not the same, in spite of attempting to choose a posteriori a closely

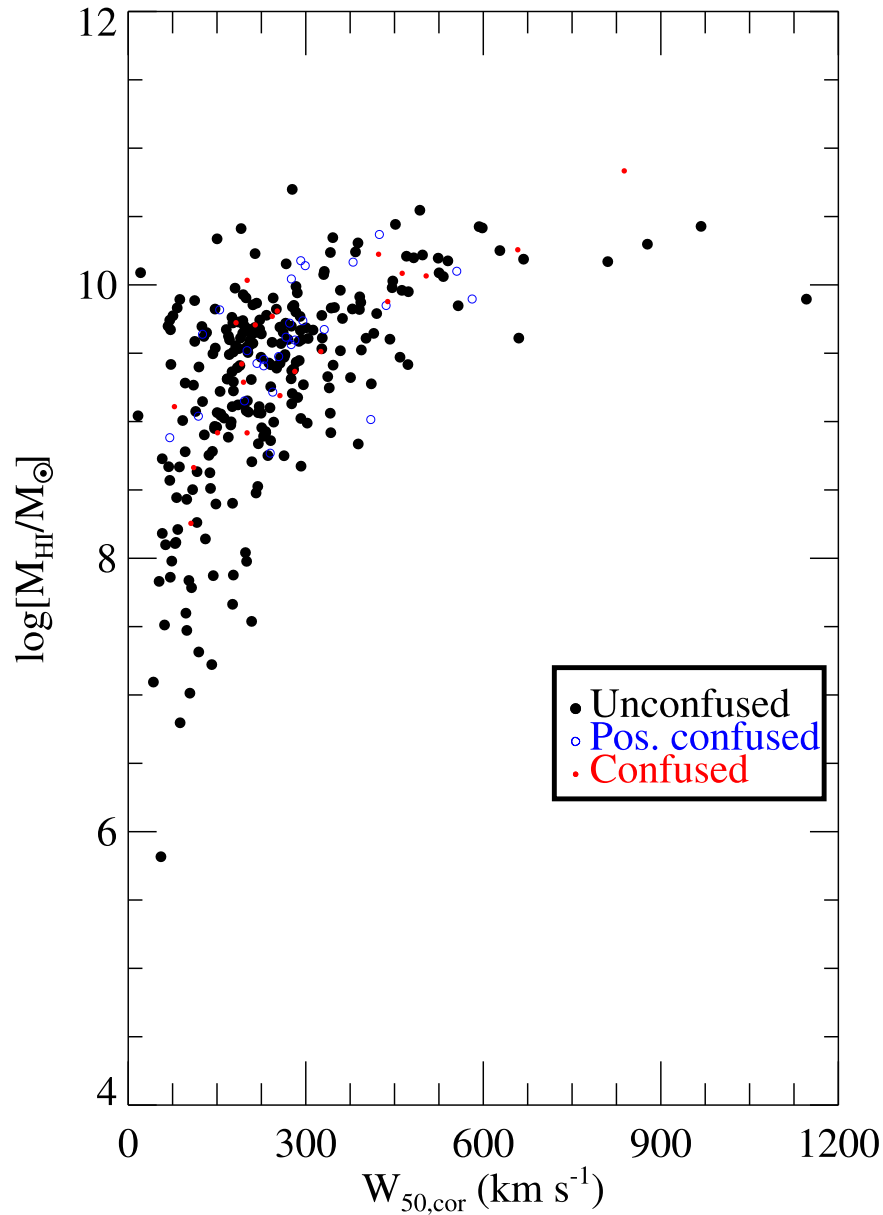


**Figure 8.** Total H I mass,  $\log(M_{\text{HI}})$  in solar masses, as a function of total mass, as represented by the inclination-corrected  $W_{50,\text{cor}}$  H I line velocity width (in kilometers per second) for the detected galaxies in our combined sample. As indicated in the legend, colors indicate the probability of a detection being confused by another galaxy within the telescope beam: black for uncontaminated, blue for possibly contaminated, and red for likely contaminated.

matched galaxy sample. Confirming this, a two-sample Kolmogorov–Smirnov test of the probability for HI masses coming from the same distribution indicates a  $46\% \pm 6\%$  probability for the HyperLeda and BGC samples, and only a  $15\% \pm 13\%$  probability for the UGC and BGC samples.

Also in terms of the total galaxy mass indicator  $W_{50}$  the distributions of the three samples show little similarity (Figure 11), like for their HI mass distributions. Here, the HIPASS bright galaxies distribution contains fewer lower total mass galaxies than either the HyperLeda or UGC samples. Again the two-sample Kolmogorov–Smirnov test bears this out, giving only a  $0\% \pm 19\%$  chance the HyperLeda and BGC samples are from the same pool, and a  $72\% \pm 8.4\%$  chance for the UGC and BGC samples. Please note that  $W_{50}$ , and not the inclination-corrected line width  $W_{50,\text{cor}}$ , was used as the HIPASS BGC does not include inclination information.

The noted differences in the total HI mass between the three samples are unsurprising, as the UGC and HyperLeda samples consist of galaxies that were not detected by previous HI surveys. That is, our samples are not unbiased and certainly do not consist of HI bright sources. The differences in dynamical mass indicator  $W_{50}$  between the three samples should also not be surprising: for a given HI mass a source with a smaller dynamic mass will tend to have a narrower HI line profile and thus a higher HI peak flux density, and will therefore be more likely to be included in the HI BGC of the HIPASS blind HI line survey.

## 6. Massive LSB Galaxies?

The impetus behind this project was to look for massive LSB galaxies and to study the properties of these systems. The obvious question, then is—how many massive LSB galaxies

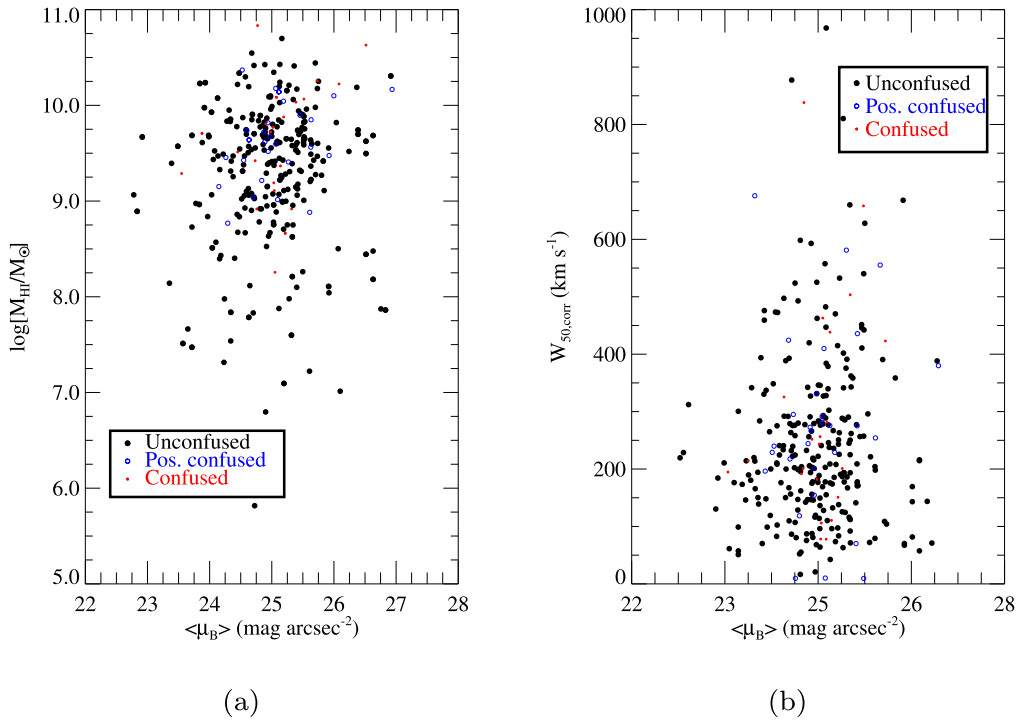


**Figure 9.** Plotted as a function of mean blue surface brightness,  $\langle\mu_B\rangle$  in magnitude per arcsecond<sup>2</sup>, are (a) the total H I mass,  $\log(M_{\text{HI}})$  in solar masses, and (b) the inclination-corrected  $W_{50,\text{cor}}$  H I line width in kilometers per second, for the detected galaxies in our combined sample. As indicated in the legend, colors indicate the probability of a detection being confused by another galaxy within the telescope beam: black for uncontaminated, blue for possibly contaminated, and red for likely contaminated.

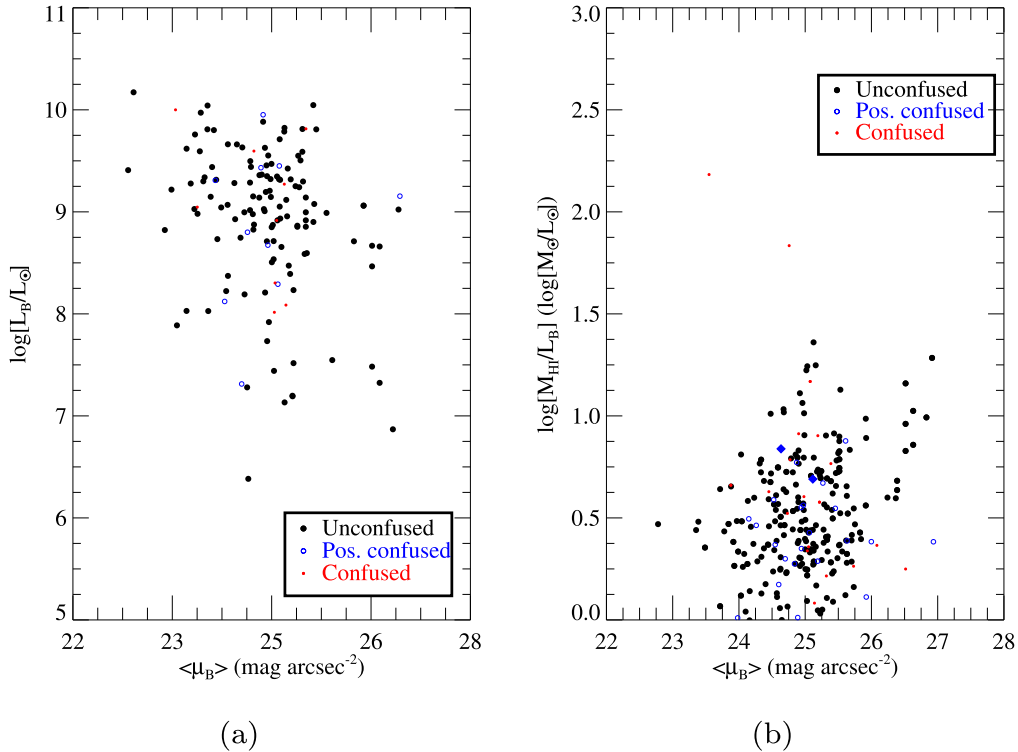


**Figure 10.** Plotted as a function of mean blue surface brightness,  $\langle\mu_B\rangle$  (in magnitude per arcsecond<sup>2</sup>), are (a) the blue luminosity,  $\log(L_B)$  in  $L_{\odot,B}$  and (b) the  $\log(M_{\text{HI}}/L_B)$  H I mass-to-light ratio, in solar units, for the galaxies in our combined sample. As indicated in the legend, colors indicate the probability of a detection being confused by another galaxy within the telescope beam: black for uncontaminated, blue for possibly contaminated, and red for likely contaminated.

were detected in this search, and can any conclusions be drawn regarding this sample from our observations?

The initial question of how many massive LSB galaxies were found must be answered in two parts. First is the question of how

many truly massive galaxies were found, and second is where or not these massive systems contain significant LSB disks.

Looking at the mass of the galaxies, in terms of their total H I gas mass we find that of the 253 uncontaminated galaxy

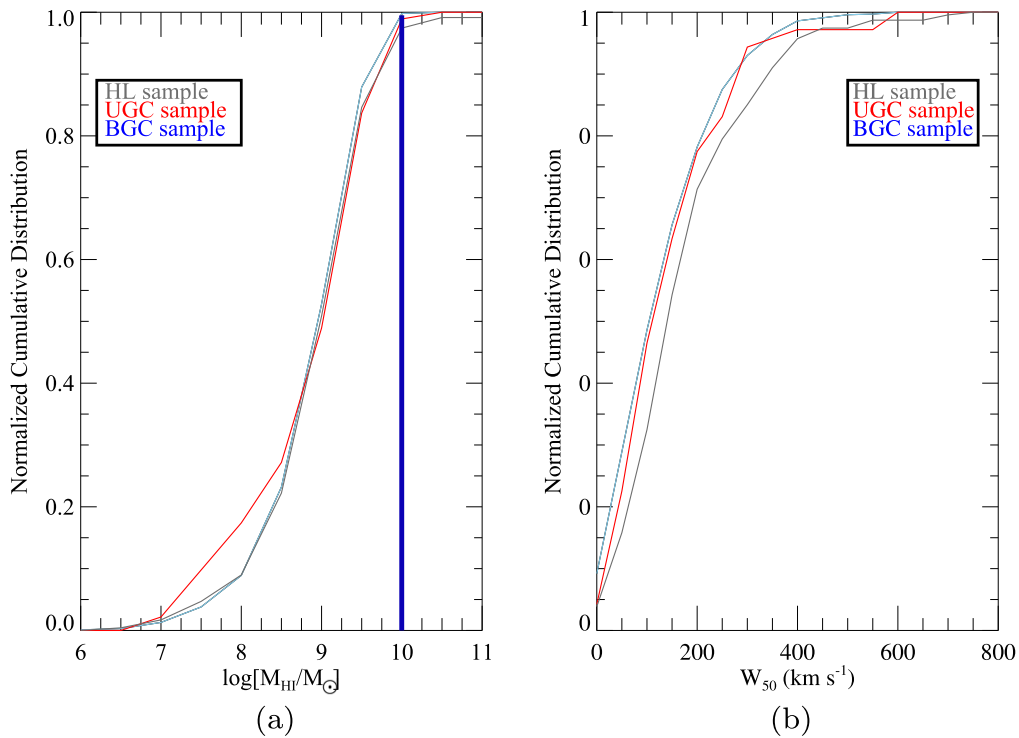


**Figure 11.** Comparison of the cumulative distributions of our two galaxy samples (HyperLeda in black, UGC in red) and the HIPASS BGC (blue) with (a) total H I mass,  $\log(M_{\text{HI}})$  in solar masses, and (b) total dynamical mass, as represented by the measured  $W_{50}$  H I line width, uncorrected for inclination. The blue vertical line in (a) shows the massive LSB galaxy limit.

detections in the survey, 189 (64.1%) have  $M_{\text{HI}} > 10^9 M_{\odot}$ , while 35 (11.9%) of these are massive in H I, with  $M_{\text{HI}} > 10^{10} M_{\odot}$ . We can also expand the definition of massive galaxy to include those with high dynamical masses, based on their inclination-corrected H I line velocity widths  $W_{50,\text{cor}}$ . We find that of the uncontaminated detections, 30 have  $W_{50,\text{cor}} \geq 500 \text{ km s}^{-1}$ . Eliminating the overlapping galaxies in these two lists gives a total of 45 massive galaxies.

Determining the central surface brightness of these galaxies from literature data is not currently possible, but we can check  $\langle \mu_{\text{B}} \rangle$ . Of the 35 uncontaminated galaxies with  $M_{\text{HI}} > 10^{10} M_{\odot}$ , 31 also have  $\langle \mu_{\text{B}} \rangle \geq 24 \text{ mag arcsec}^{-2}$ . Of the 30 uncontaminated galaxies with  $W_{50,\text{cor}} \geq 400 \text{ km s}^{-1}$ , 30 have  $\langle \mu_{\text{B}} \rangle \geq 24 \text{ mag arcsec}^{-2}$ . Finally, 20 galaxies have  $M_{\text{HI}} > 10^{10} M_{\odot}$ ,  $W_{50,\text{cor}} \geq 500 \text{ km s}^{-1}$ , and  $\langle \mu_{\text{B}} \rangle \geq 24 \text{ mag arcsec}^{-2}$ . All of these are clearly worthy of follow-up observations in the optical and radio to understand their properties better.

## 7. Conclusions

While the intent of this survey was to identify massive LSB galaxies, it is very instructive to look at the overall mass distribution of the sample. The average H I mass of the (uncontaminated) sample is  $10^{9.35 \pm 0.04} M_{\odot}$ , and their average velocity width  $\langle W_{50,\text{cor}} \rangle$  is  $199 \pm 7 \text{ km s}^{-1}$ , reinforcing the fact that LSB galaxies have the same mass distribution as their HSB counterparts and are not preferentially dwarf systems.

Of more interest will be follow-up H I radio synthesis and optical surface photometry observations of these galaxies. Mapelli et al. (2008) have shown that at least some of the massive LSB galaxies are formed through the interaction and merger of smaller galaxy systems. This sample will provide an excellent test case to determine if there is indeed a mass beyond which all LSB galaxies are formed through interactions and

mergers or if, like their HSB counterparts, these systems follow a variety of paths to reach their current state.

This material is based upon work supported by the Green Bank Observatory which is a major facility funded by the National Science Foundation operated by Associated Universities, Inc. This research has made use of the NASA/IPAC Extragalactic Database (NED), which is funded by the National Aeronautics and Space Administration and operated by the California Institute of Technology; the HyperLeda database (<http://leda.univ-lyon1.fr>); SDSS-II data (<http://www.sdss3.org>), which has been provided by the Alfred P. Sloan Foundation, the Participating Institutions, the National Science Foundation, and the U.S. Department of Energy Office of Science; and POSS-II data, which were produced at the Space Telescope Science Institute under U.S. Government grant NAG W-2166 based on photographic data obtained using the Oschin Schmidt Telescope on Palomar Mountain and the UK Schmidt Telescope. The Arecibo Observatory is operated by SRI International under a cooperative agreement with the National Science Foundation (AST-1100968), and in alliance with Ana G. Méndez-Universidad Metropolitana, and the Universities Space Research Association. The Nançay Radio Observatory is operated by the Paris Observatory, associated with the French Centre National de la Recherche Scientifique.

## Appendix A Notes on Individual Galaxies

### A.1. HyperLeda Galaxy Sample

#### A.1.1. CGMW 1-0409

This galaxy was not in the list of planned targets. It was however detected at the GBT in an off-source (blank sky)



spectrum used to calibrate another galaxy. Although our detection matches the Parkes' HIPASS profile (Meyer et al. 2004) in  $V_{\text{HI}}$  ( $2805 \text{ km s}^{-1}$ ) and  $W_{50}$  ( $131 \text{ km s}^{-1}$ ), our HI flux ( $8.6 \pm 0.2 \text{ Jy km s}^{-1}$ ) is much lower than the HIPASS value of  $16.1 \text{ Jy km s}^{-1}$ , indicating the source may be quite extended given the difference in the telescopes' HPBW's (GBT 8'7 and Parkes 15'5, although the Parkes' positional accuracy is typically better than 7'5; Zwaan et al. 2004).

#### A.1.2. ESO 338-020

It is likely that some of the detected flux for ESO 338-020 is from the nearby galaxy 2MASX J19412558-3820561, whose optical velocity is only  $12 \text{ km s}^{-1}$  higher and is located  $8'.3$  away from our target, ESO 338-020, on the edge of the Nançay HPBW.

#### A.1.3. ESO 368-004

ESO 368-004 has no known galaxies within  $15'$  and  $9000 \text{ km s}^{-1}$ , yet the Nançay and GBT flux measurements for this galaxy differ by  $1.6 \text{ Jy km s}^{-1}$  (12%). Follow-up GBT observations confirmed the original GBT values. Yet, as all three spectra have high S/Ns, the average of the three results was reported in Table 2. Please note, too, that the HIPASS detection of this object has an even higher flux than our three measurements (Meyer et al. 2004):  $\text{flux}_{\text{NAN}} = 12.91$ ,  $\text{flux}_{\text{GBT1,GBT2}} = 14.51$ ,  $13.45$ , and  $\text{flux}_{\text{HIPASS}} = 15.08 \text{ Jy km s}^{-1}$ .

#### A.1.4. ESO 377-045

Three marginal HI detections of ESO 377-045 with peak S/N values of 3.2 to 4.3 were reported by Matthews & Gallagher (1996) based on Green Bank 42 m telescope observations with a  $21'$  HPBW, at 1323, 2057, and  $3087 \text{ km s}^{-1}$ ; the latter has  $W_{20} = 167 \text{ km s}^{-1}$  and  $F_{\text{HI}} = 2.5 \text{ Jy km s}^{-1}$ , similar to our detection with  $V_{\text{HI}} = 3125 \text{ km s}^{-1}$ ,  $W_{20} = 171 \text{ km s}^{-1}$ , and  $F_{\text{HI}} = 2.4 \text{ Jy km s}^{-1}$ .

#### A.1.5. ESO 398-011

The galaxy ESO 398-010 is only  $12 \text{ km s}^{-1}$  away from ESO 398-011. The galaxies' east–west separation is  $8'$ , or five times the east–west Nançay beam radius. It is therefore not likely that the measured spectrum contains some contribution from ESO 398-010.

#### A.1.6. ESO 463-005

The reported optical velocity for this galaxy (Jones et al. 2009) is  $3031 \pm 45 \text{ km s}^{-1}$ , significantly ( $5\sigma$ ) different from the  $2809 \pm 3 \text{ km s}^{-1}$  HI measurement originally made with the Nançay telescope. Follow-up GBT observations, though, showed our Nançay spectrum to be likely contaminated by a nearby galaxy, NGC 6925, which was probably caught in the larger Nançay beam. The GBT observations give an HI velocity of  $3014 \text{ km s}^{-1}$ , much closer to the Jones et al. (2009) result. Only the GBT results were used for the final values (Table 2).

#### A.1.7. ESO 482-024

It is highly likely that our Nançay HI spectrum is contaminated by the galaxy NGC 1403, which is  $56 \text{ km s}^{-1}$

and  $12'.0$  away from ESO 482-024, on the edge of the Nançay beam. NGC 1403 was detected at Parkes in HIPASS (Meyer et al. 2004).

#### A.1.8. ESO 491-002

No galaxy is discernible in the DSS2 images, but a *B*-band image from Lauberts & Valentijn (1989, as displayed on NED) taken at the ESO 1 m Schmidt telescope shows an LSB object, which could be a distorted galaxy (Figure 12). We did not detect it in HI.

#### A.1.9. ESO 491-003

As the original Nançay detection of this source had a nearby (in frequency) RFI source, follow-up observations were taken. Only the more recent GBT results are reported in Table 2.

#### A.1.10. ESO 492-001

The GBT profile has a  $84 \text{ km s}^{-1}$  (40%, or  $6\sigma$ ) larger  $W_{50}$  line width than our Nançay profile, and a 22% ( $3.6\sigma$ ) higher integrated flux. As there are no neighbors within either telescope beam, it is likely the higher S/N GBT measurements are more reliable than the Nançay values. Subsequent GBT observations agreed with the initial GBT values, and we therefore used only the GBT values used for Table 2.

#### A.1.11. ESO 501-029

It appears possible that nearby galaxy UGCA 212 has contaminated our GBT HI detection of our target, ESO 501-029. UGCA 212 is  $28 \text{ km s}^{-1}$  and  $11'.2$  (2.6 times the GBT beam radius) away from our target and its published Parkes (HPBW =  $15'.5$ ) HIPASS profile (Meyer et al. 2004) shows  $V_{\text{HI}} = 1042 \text{ km s}^{-1}$ ,  $W_{50} = 63 \text{ km s}^{-1}$ , and  $F_{\text{HI}} = 29.4 \text{ Jy km s}^{-1}$ , or 7.5 times our flux measured toward ESO 501-029.

#### A.1.12. ESO 540-030

A weak HI detection of ESO 540-030 was reported by Bouchard et al. (2005) in Parkes single-dish spectra and Australia Telescope Compact Array (ATCA) images at  $V_{\text{HI}} = 233 \text{ km s}^{-1}$ , with  $W_{50} = 26 \text{ km s}^{-1}$  and  $F_{\text{HI}} = 0.33 \text{ Jy km s}^{-1}$ . This low velocity is consistent with the distance of  $3.2 \text{ Mpc}$  estimated from surface brightness fluctuations by Jerjen et al. (1998). Our Nançay data show a  $7 \text{ mJy}$ ,  $S/N = 3.3$  peak near the Parkes velocity, which is too weak for a confirmation. Follow-up observations with the GBT indicate no signal, with an rms of  $1.8 \text{ mJy}$ , compared to the 6.5 times higher  $\sim 12 \text{ mJy}$  peak reported by Bouchard et al. (2005). The GBT data confirm that the Bouchard et al. (2005) detection was spurious. Similarly, we also consider the low  $S/N = 3.3$  signal seen by Nançay at  $8093 \text{ km s}^{-1}$  to be spurious, as it was also not seen by the GBT.

#### A.1.13. IC 3852

There are no known galaxies within  $15'$  and  $8000 \text{ km s}^{-1}$  of IC 3852, yet the differences between the fluxes measured at Arecibo and the two GBT measurements is large (2.7 and  $3.2/3.4 \text{ Jy km s}^{-1}$ , respectively) as are the differences in velocity widths ( $W_{50} = 203$  and  $205/222 \text{ km s}^{-1}$ , respectively). Published Arecibo data (Springob et al. 2005; Haynes et al. 2018) show  $V_{\text{HI}} = 4375 \text{ km s}^{-1}$ ,  $W_{50} = 198 \text{ km s}^{-1}$ , and

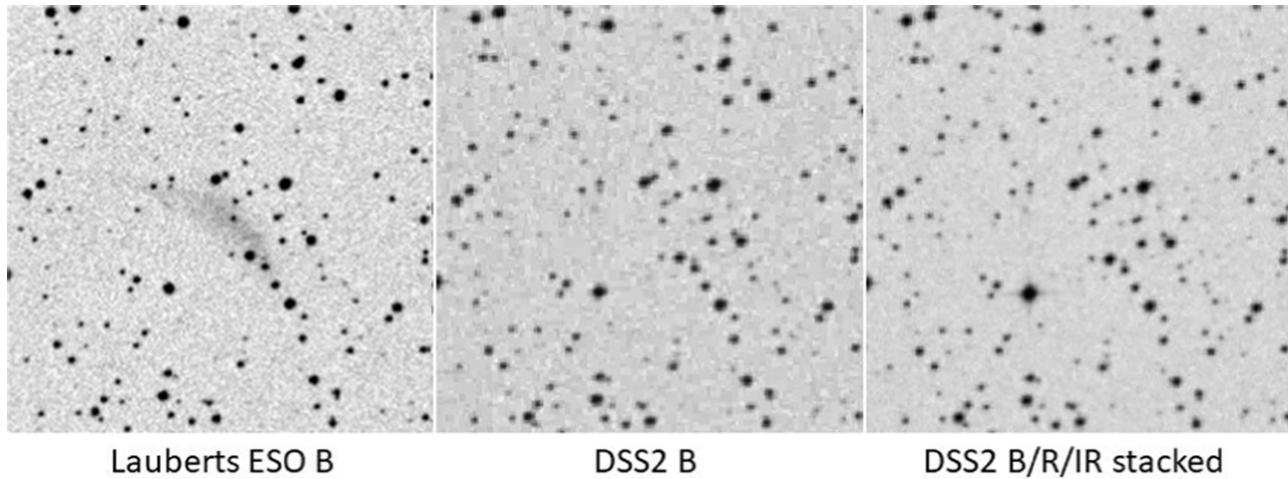


**Figure 12.** Optical images of ESO 491-002. A  $B$ -band image (left) from Lauberts & Valentijn (1989) taken at the ESO 1 m Schmidt telescope shows an LSB object, which could be a distorted galaxy, but no galaxy is discernible on the DSS2  $B$ ,  $R$ , or  $IR$  images (Abazajian et al. 2004) taken with the 1.2 m Palomar Schmidt telescope. Images are  $4\prime3 \times 4\prime3$  in size.

$F_{\text{HI}} = 3.75 \text{ Jy km s}^{-1}$ . With no clear reason for the differences, the average of our observations are listed in Table 2.

#### A.1.14. PGC 2582

The velocity of our GBT detection for PGC 2582 at  $15,050 \text{ km s}^{-1}$  does not match those of the two galaxies within the telescope beam with measured optical velocities, 2MASXJ00430067-0913463 at  $29,310 \text{ km s}^{-1}$  (Christlein & Zabludoff 2003) and WISEA J004314.24-091247.0 at  $22,892 \text{ km s}^{-1}$  (Moretti et al. 2017). It is likely our detection of HI is actually from the Abell 85 cluster in the region, which has a mean velocity of  $16,500 \text{ km s}^{-1}$  and a velocity dispersion of  $1100 \text{ km s}^{-1}$  (Oegerle & Hill 2001). Unfortunately, RFI prevented the GBT observations from reliably detecting any HI at or near the optical velocities measured for the two galaxies within the telescope beam.

#### A.1.15. PGC 3843

The HI profile measured at the GBT for PGC 3843 is quite broad ( $W_{50} = 403 \text{ km s}^{-1}$ ). No previous redshift has been reported for PGC 3843, and there are no other galaxies within the GBT beam with velocities within  $\pm 500 \text{ km s}^{-1}$  of  $14,367 \text{ km s}^{-1}$ , the central velocity of PGC 3843's HI detection. However, two galaxies, WISEA J010444.68-110422.9 and MCG-02-03-071, lie on either side of PGC 3843,  $7'$  and  $12'$  away, respectively, and at  $14,243$  and  $14,084 \text{ km s}^{-1}$ , respectively (Figure 13). It is possible that PGC 3843 has had a recent encounter with (one of) its neighbors, resulting in its disturbed optical morphology and its exceptionally large HI line width. Follow-up observations will be required to determine if this is the case.

#### A.1.16. PGC 7225

Zabludoff & Mulchaey (1998) give an optical velocity of  $5071 \pm 80 \text{ km s}^{-1}$ , which is  $123 \text{ km s}^{-1}$  lower than that found by us in HI, but its high uncertainty, combined with our independent detections at Nançay and GBT, makes it likely our measurement is a more accurate value for the average velocity of the galaxy.

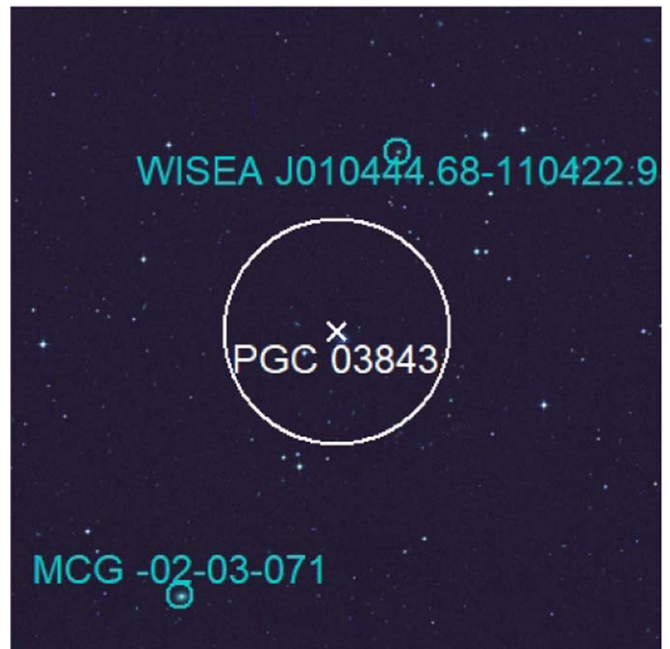


**Figure 13.** DSS multicolor (IR, red, and blue plates) image of PGC 3843 (center, white cross). The large white circle shows the  $8\prime7$  GBT beam, and the cyan circles denote the two galaxies which have likely recently interacted with PGC 3843, WISEA J010444.68-110422.9 and MCG-02-03-071. The image is  $25'$  across.

#### A.1.17. PGC 16370

Using the Westerbork Synthesis Radio Telescope (WRST), Ramatsoku et al. (2016) also measured PGC 16370's HI properties. Their results for  $V_{\text{HI}}$  and  $W_{50}$  match those we found, but their integrated flux value is only 60% of that found by our original low S/N Nançay detection. However, our much higher S/N GBT follow-up observations confirm the WRST data, and are consequently listed in Table 2.

#### A.1.18. PGC 17124

A potential source of confusion is the galaxy UGC 3276, which lies  $9\prime1$  from PGC 17124, i.e., inside the NRT HPBW

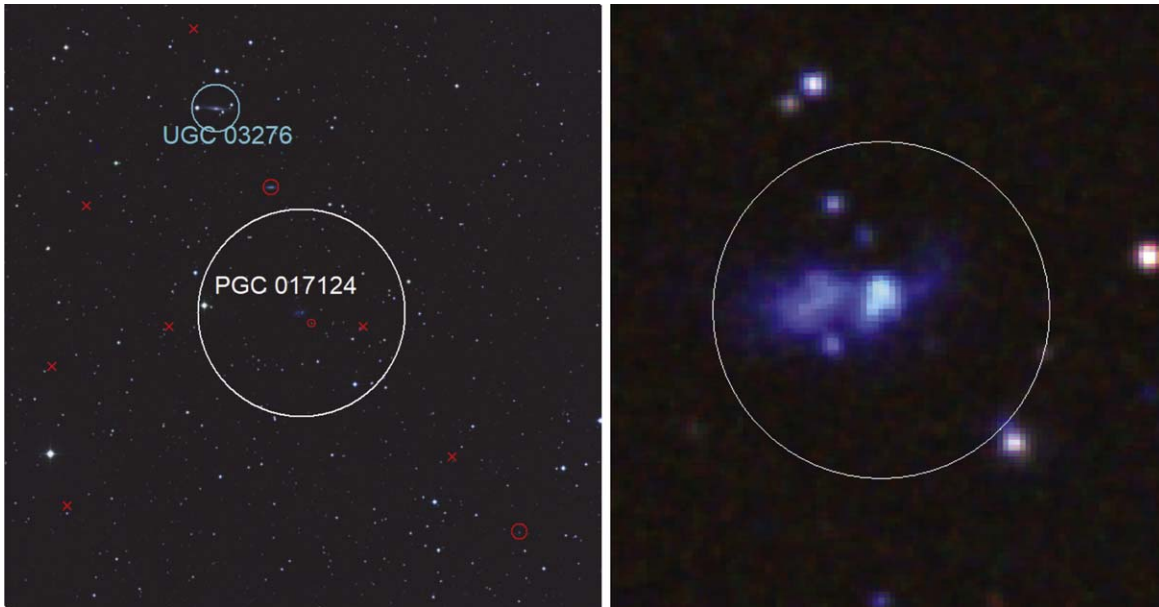


**Figure 14.** DSS multicolor (IR, red, and blue plates) images of PGC 17124 (center,  $30''$  white circle). Left: the large white circle shows the  $8'7$  GBT beam, and UGC 3276 is denoted by the ( $60''$ ) cyan circle. The two galaxies with known velocities more than  $2000 \text{ km s}^{-1}$  from that of PGC 17124 are denoted by red circles, while the three previously identified galaxies without known velocities are denoted by red crosses. The image is  $25'$  across. Right: enlargement, showing the disturbed morphology of PGC 17124.

but outside the GBT beam (see Figure 14). Therefore, our GBT profile of PGC 17124 is unlikely to be contaminated by its neighbor and we used its line parameters in Table 2. Measurements centered on UGC 3276 with the National Radio Astronomy Observatory’s 300 foot telescope (Springob et al. 2005) and Jodrell Bank’s 76 m Lovell telescope (Lang et al. 2003) give HI profile parameters consistent with our observations:  $V_{\text{HI}} = 2490 \text{ km s}^{-1}$ ,  $W_{50} = 270 \text{ km s}^{-1}$ , and  $F_{\text{HI}} = 15.3 \text{ Jy km s}^{-1}$ . The beam radii of the two telescopes are more than two times smaller than the separation between the two galaxies, so it is unlikely that these profiles are contaminated by our target galaxy, PGC 17124. As can also be seen in Figure 14, the morphology of PGC 17124 is clearly disturbed. It is quite possible, then, that UGC 3276 and PGC 17124 have had at least one encounter in the recent past.

#### A.1.19. PGC 21133

There is a  $90 \text{ km s}^{-1}$  difference between our Nançay and GBT  $W_{50}$  line widths, but the  $W_{20}$  values are comparable. However, this difference is not really significant given the estimated uncertainty in the  $W_{50}$  value of the lower S/N Nançay data. Both observations are averaged in Table 2.

#### A.1.20. PGC 21529

At  $3/4$  from PGC 21529 ( $V_{\text{opt}} = 4059 \pm 2 \text{ km s}^{-1}$ ) lies KUG 0737+323 with a  $138 \text{ km s}^{-1}$  lower  $V_{\text{opt}}$  of  $3921 \pm 3 \text{ km s}^{-1}$  (Alam et al. 2015). Both our Nançay and GBT spectra likely include both PGC 21529 and KUG 0737+323, whereas due to its smaller  $3/6$  beam size the Arecibo data appear to be unaffected by KUG 0737+323. As a result, only the Arecibo result is listed in Table 2.

#### A.1.21. PGC 21907

The intended target of this survey was PGC 21907. However observations taken after our survey, including optical velocity

measurements, have shown it to be two distinct galaxies—KUG 0746+398A (the foreground LSB galaxy) and KUG 0746+398B (aka PGC 21907—a background spiral galaxy). Including these two objects, there are a total of eight galaxies with known redshifts within the GBT beam when it was pointed toward PGC 21907, all of which have published redshifts (Table 7 & Figure 15). Four of these have redshifts within the frequency range of our GBT observations, whereas the others lie far outside it. Of these four, our GBT observations detected HI gas at the redshift of SDSS J074933.51+394424.3 only. A possible detection was seen at  $12,420 \text{ km s}^{-1}$  (KUG 0746+398A), but there were significant baseline issues, making the detection uncertain. No HI emission was detected at the velocities of KUG 0746+398A, KUG 0746+398B (aka PGC 21907), or SDSS J074939.55+394316.7.

#### A.1.22. PGC 23328

PGC 23328 is listed as member of a small group of galaxies by both Tempel et al. (2017) and Tempel et al. (2012); see Table 8. This group includes, at minimum, PGC 23328, WISEA J081923.48+252621.4, and WISEA J081955.30+252733.0, but it is likely that KUG 0816+256B is also part of this group. However, as none of the galaxies in this group were included in the telescope beams, it is likely the measured HI flux belongs only to PGC 23328 (Figure 16).

#### A.1.23. PGC 23879

PGC 23879 has one companion, LEDA 3097429, which lies  $11/5$  but only  $27 \text{ km s}^{-1}$  away. There are two additional galaxies, ASK 151063.0 and ASK 151084.0, which lie  $13/1/1675 \text{ km s}^{-1}$  and  $8/6/1721 \text{ km s}^{-1}$  away, respectively. As the HI spectrum of PGC 23879 was taken with the GBT, which has a beam size of  $9/2$  at the frequencies of interest, it is possible that it contains some HI gas from LEDA 3097429. It is highly unlikely that gas was detected from the other galaxy



**Table 7**  
All Galaxies with Known Redshifts Within the GBT Beam When Pointed at PGC 21907

Object	Velocity ( $\text{km s}^{-1}$ )	GBT Det? (Y/N)	GBT rms (mJy)	Vel. Ref.
SDSS J074933.51+394424.3	2943	Y	3.2	5, 8, 9, 10
KUG 0746+398A	12,420	Y	2.2	2
PGC 21907	$22,210 \pm 4500$	N	1.8	1
SDSS J074939.55+394316.7	12,536	N	2.2	3, 4, 5, 6
WISEA J074940.39+394604.7	28,603	N	N/A	2, 5, 6, 10
WISEA J074945.78+394354.4	46,750	N	N/A	5, 6, 10
WISEA J074949.97+393945.9	151,577	N	N/A	10
WISEA J074951.56+393934.9	150,496	N	N/A	10

**Note.** Velocity references: (1) Berlind et al. (2006); (2) Bilicki et al. (2014); (3) Alatalo et al. (2016); (4) Galloway et al. (2015); (5) Abazajian et al. (2004); (6) Abazajian et al. (2003); (7) Kourkchi & Tully (2017); (8) van Driel et al. (2016); (9) Alam et al. (2015).

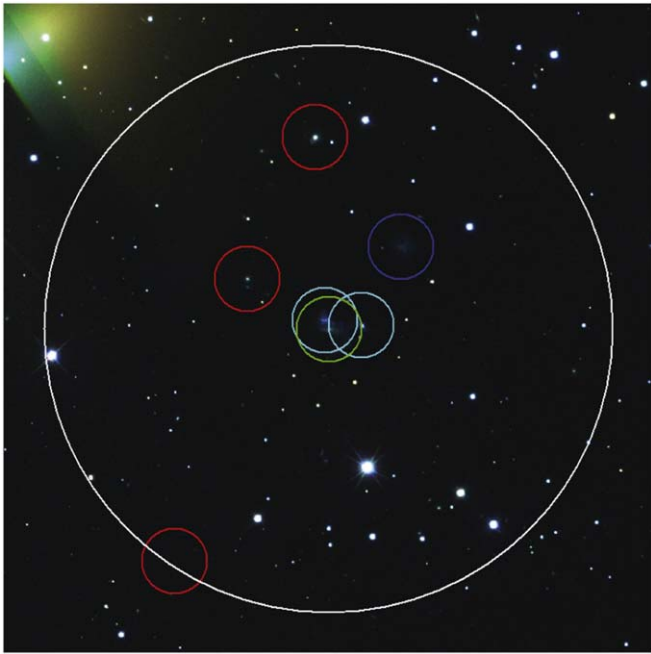


**Figure 15.** SDSS DR12 false color (*i*, *r*, and *g* filters) image of the galaxies with known redshifts lying within the GBT beam centered on PGC 21907 (cyan circle). The large white circle shows the 8' GBT beam. The blue circle denotes the nearest galaxy, SDSS J074933.51+394424.3, the two cyan circles denote galaxies KUG 0746+398A (left) and SDSS J074939.55+394316.7 (right), the green circle PGC 21907 (aka KUG 0746+398B), and the red circles denote the three Wide-field Infrared Survey Explorer (WISE) galaxies which lie outside our redshift detection range. The image is 9'0 across.

pair, but it is worth noting them nonetheless, as the four galaxies could form a loose group.

#### A.1.24. PGC 26708

This galaxy is part of the PGC 26708–NGC 2883 pair of galaxies, making it difficult to know which fraction of the measured HI flux can be attributed to our target, PGC 26708.

#### A.1.25. PGC 26936

The galaxy SDSS J092844.48+351641.3 is 11'.9 and 48  $\text{km s}^{-1}$  away from our target, PGC 26936. As the larger Nançay beam does not show either a larger  $W_{50}$  or line flux

than we observed at Arecibo, it is highly unlikely that our spectra of our target are contaminated.

#### A.1.26. PGC 27485

We observed PGC 27485 at Nançay, Arecibo, and the GBT. Comparing the measured HI profiles it appears that the smaller Arecibo beam did not observe all of the extended HI of this north–south oriented galaxy (the line flux measured at Arecibo is 29% lower than at Nançay;  $\text{flux}_{\text{AO}} = 4.29 \pm 0.07$ ;  $\text{flux}_{\text{NAN}} = 5.98 \pm 0.26$ ;  $\text{flux}_{\text{GBT}} = 6.29 \pm 0.12 \text{ Jy km s}^{-1}$ ). However without a full map of the galaxy's gas distribution we cannot know this for certain and listed the average of both values in Table 2.

#### A.1.27. PGC 27849

Although its  $V_{\text{HI}}$  values found with the three telescopes are highly consistent, the values measured for  $W_{50}$ ,  $W_{20}$ , and the HI flux vary significantly. The GBT values are the largest, with  $\log(M_{\text{HI}}/M_{\odot}) = 9.88$  and 10.05 ( $W_{20} = 393/332$  and  $W_{50} = 357$  & 312) while the Arecibo and Nançay observations are similar, with  $\log(M_{\text{HI}}/M_{\odot}) = 9.60$  and 9.73 ( $W_{20} = 247$  & 236 and  $W_{50} = 221$  & 197), respectively. There are, however, no known galaxies within 14' and 2000  $\text{km s}^{-1}$  from our target PGC 27849, nor are there any clear, unidentified neighbors. It is therefore unclear what the origins are of the additional flux measured by the GBT.

Results from all four sets of observations are shown in Table 3 and also in Figure 1, with the older GBT observation shown in light blue. The results in Table 2 are averaged from all four sets of observations.

#### A.1.28. PGC 28799

The GBT data show a clear detection of HI emission at 4526  $\text{km s}^{-1}$  with a second (marginal) detection at  $\sim 6130 \text{ km s}^{-1}$ . These velocities do not, however, match the 7313  $\text{km s}^{-1}$  found for the HI source HIPASS J0958-38 (Meyer et al. 2004; Doyle et al. 2005). Another galaxy, WISEA J095813.16-380926.6, lies 4'.5 from our target PGC 28799 and has an optical velocity of  $7234 \pm 45 \text{ km s}^{-1}$  (Jones et al. 2009) Neither of these redshifts match those found in our survey, and no HI emission was found at either of these velocities.



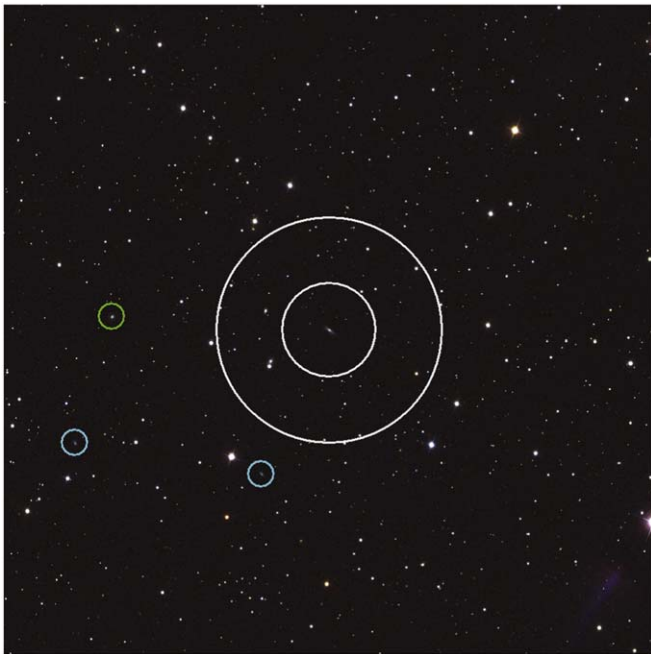


**Figure 16.** SDSS DR12 false color ( $i$ ,  $r$ , and  $g$  filters) image of the PGC 23328 galaxy group. The white circles show the 8.7 GBT beam and the 3.6 Arcsec beam centered on PGC 2338. The other two known members of the group, WISEA J081955.30+252733.0 and WISEA J081923.48+252621.4, are denoted by cyan circles (listed from left to right in the image). The fourth potential group member, KUG 0816+256B, is denoted by the green circle. The image is 25' across.

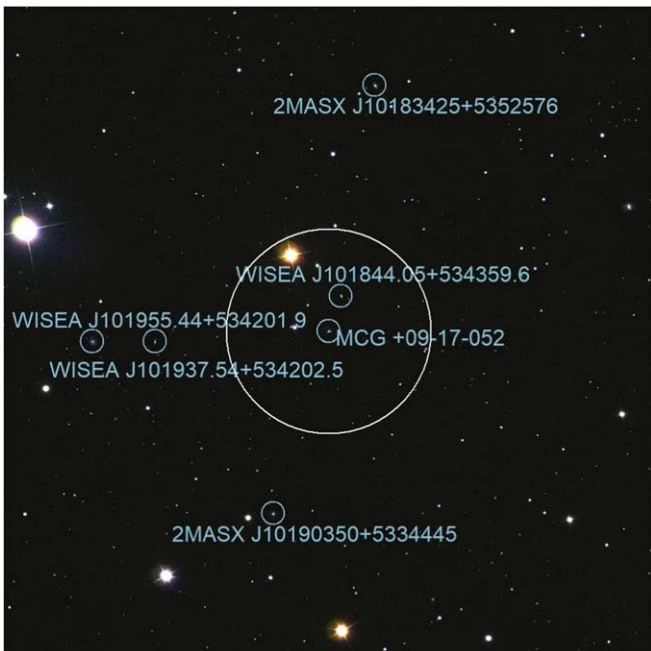


**Figure 17.** SDSS DR12 false color ( $i$ ,  $r$ , and  $g$  filters) image of the PGC 30113 galaxy group. The large white circle shows the 8.7 GBT beam. The six known group members are denoted by cyan circles. The image is 27.5' across.

#### A.1.29. PGC 29681

It is possible, though not likely, that our Nançay spectrum of our target PGC 29681 is contaminated by two nearby galaxies, UGC 5485 and SDSS J101131.31+650524.7, which are within

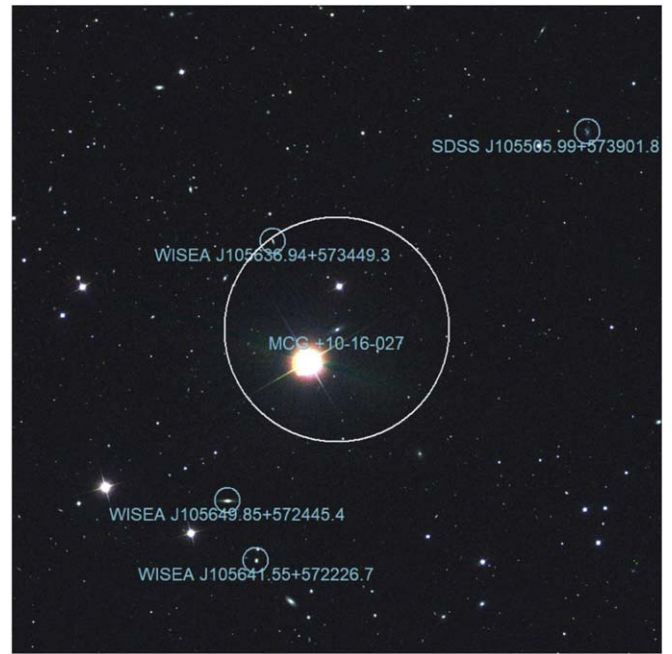


**Figure 18.** SDSS DR12 false color ( $i$ ,  $r$ , and  $g$  filters) image of the PGC 32862 galaxy group. The large white circle shows the 8.7 GBT beam. The four known group members are denoted by cyan circles. The image is 25.5' across.

**Table 8**  
Galaxies in the PGC 23328 Group

Object	Velocity ( $\text{km s}^{-1}$ )	Vel. References
PGC 23328	5829	1,2,3
WISEA J081923.48+252621.4	5770	1,2,3
WISEA J081955.30+252733.0	6006	1
KUG 0816+256B	7316	1,2,3

**Note.** Velocity references: (1) Alam et al. (2015); (2) Haynes et al. (2018); (3) Haynes et al. (2011).

**Table 9**  
Galaxies in the PGC 30113 Group

Object	Velocity ( $\text{km s}^{-1}$ )	Vel. References
PGC 30113	13,491	1, 2, 3, 4, 5
2MASX J10183425+5352576	13,607	1, 2, 4, 5
WISEA J101844.05+534359.6	14,159	1, 4, 5
WISEA J101937.54+534202.5	14,169	1, 4, 5
WISEA J101955.44+534201.9	14,269	1, 2, 5
2MASX J10190350+5334445	15,137	1, 4, 5

**Note.** Velocity references: (1) Alam et al. (2015); (2) Galloway et al. (2015); (3) Kruk et al. (2018); (4) Bilicki et al. (2014); (5) Abazajian et al. (2004).

8.5 and 58  $\text{km s}^{-1}$  (SDSS optical velocities) from our target. Of the three, UGC 5485 is by far the brightest, by about 2 mag in  $B$ . It was observed in H I at Effelsberg and Nançay (Huchtmeier 1997; van Driel et al. 2000), and its separation from our target is, respectively, 1.3 and 3.5 times the beam radius for

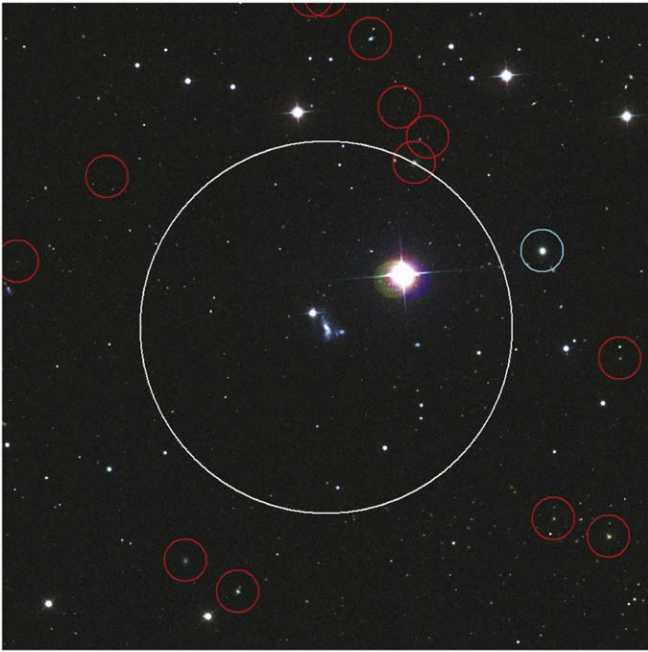


**Figure 19.** SDSS DR12 false color (*i*, *r*, and *g* filters) image of PGC 38698 (center). The large white circle shows the 8'7 GBT beam. The galaxy I Zw 031 is denoted by the cyan circle on the right and the known background galaxies by red circles. The image is 15' across.

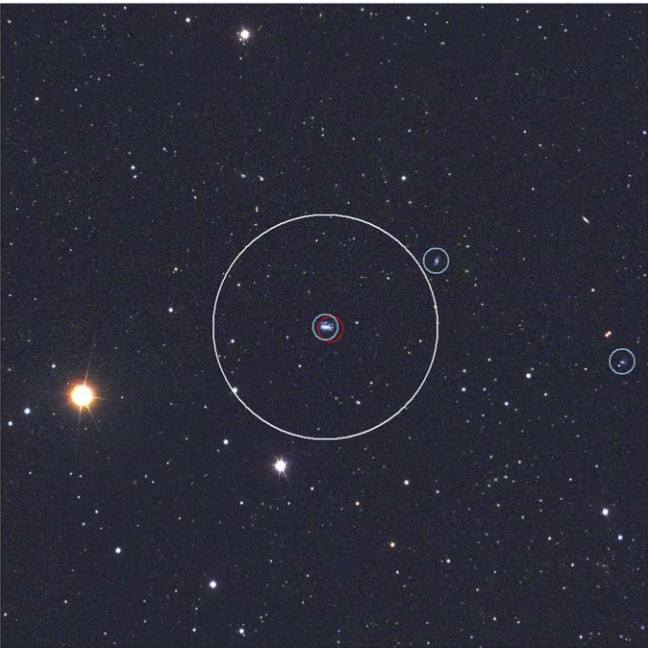


**Figure 20.** SDSS DR12 false color (*i*, *r*, and *g* filters) image of our target galaxy PGC 43880 (center, cyan circle). The large white circle shows the 8'7 GBT beam. The position of SDSS J125405.61+481534.9 is denoted by the red circle, close to our target, while WISEA J125341.21+481813.1 (top center) and WISEA J125257.97+481417.6 (on the right) are denoted by cyan circles. The image is 25' across.

the Effelsberg and Nançay telescopes. The Nançay profiles of our target and UGC 5485 are therefore not likely to be contaminated by each other. The Effelsberg and NRT profiles of UGC 5485 are similar in  $V_{\text{HI}}$ , 5987 km s<sup>-1</sup>, and  $F_{\text{HI}}$ , 15 Jy km s<sup>-1</sup> (i.e., almost 4 times of that of our target), but the Nançay  $W_{50}$  of 331 km s<sup>-1</sup> is 65 km s<sup>-1</sup> broader.

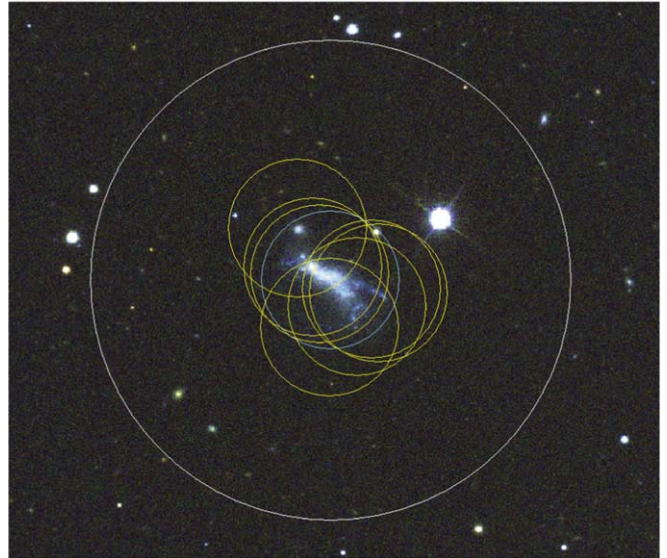


**Figure 21.** SDSS DR12 false color (*i*, *r*, and *g* filters) image of PGC 51872 (center, cyan circle). The white circle shows the 3'6 Arecibo beam. The yellow circles denote the various galaxies listed in Table 11, which we believe to be part of PGC 51872 rather than separate galaxies.

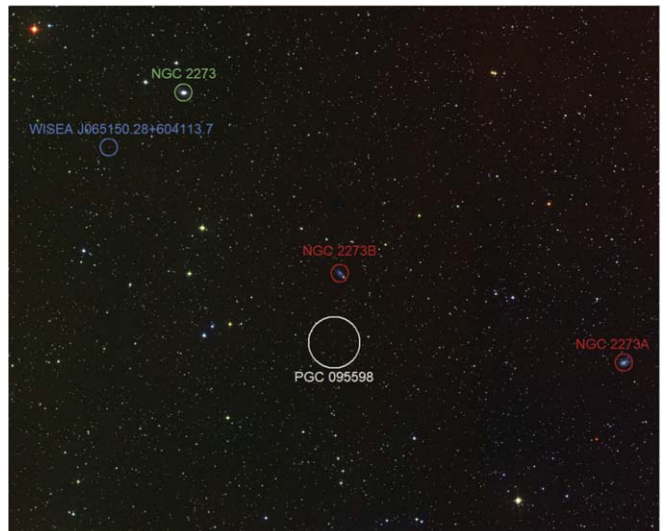


**Figure 22.** DSS false color (IR, red, and blue plates) image of the NGC 2273 galaxy group, which likely includes our target galaxy PGC 95598—inside the large white circle showing the 8'7 GBT beam. The four other circles denote the known group members, with their color indicating the object's relative velocity within the group. The image is 110'0 × 90'0 across.

#### A.1.30. PGC 30113

It is highly likely that our measured HI flux for PGC 30113 is contaminated by other galaxies. It is part of a small group of galaxies within approximately 14' and 2500 km s<sup>-1</sup> from each other (Figure 17 and Table 9). Likely due to its group membership, past observations have found a large range of redshifts for PGC 30113, from 10,983 km s<sup>-1</sup> (Kruk et al. 2018) to 21,203 km s<sup>-1</sup> (Bilicki et al. 2014), but the majority of observations give 13,401 ± 7 km s<sup>-1</sup> (Abazajian et al. 2004; Bilicki et al. 2014; Alam et al. 2015; Galloway et al. 2015), consistent with our GBT value of 13,402 km s<sup>-1</sup>.



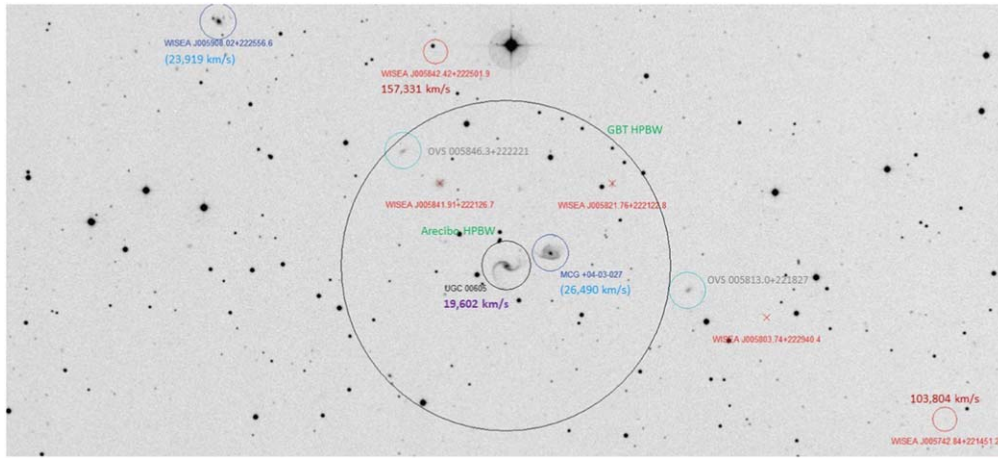


**Figure 23.** DSS blue image of UGC 605 showing the 3/6 Arcicibo and 8/7 GBT beams as black circles. The galaxies possibly related to the H I spectra detected when observing UGC 605 are denoted by the cyan circles. Other galaxies are denoted in dark blue and red.

**Table 10**  
Galaxies in the PGC 32862 Group

Object	Velocity (km s <sup>-1</sup> )
PGC 32862	13,973
SDSS J105505.99+573901.8	13,839
WISEA J105636.94+573449.3	13,968
WISEA J105649.85+572445.4	14,031

**Note.** Velocity reference: Albareti et al. (2017).

**Table 11**  
Galaxies Likely Misidentified as Separate from PGC 51872

Object	Velocity (km s <sup>-1</sup> )	Vel. References
GALEXMSC J143103.29+353112.0	3897	(1)
WISEA J143104.15+353132.1	3897	(2)
SDSS J143103.66+353115.8	4067	(3)
SDSS J143102.07+353058.6	4117	(4)
SSTSL2 J143101.52+353105.9	3298	(5)
SDSS J143103.06+353049.7	4179	(5)
SDWFS J143101.34+353104.7	4197	(1)

**Note.** Velocity references: (1) Kozłowski et al. (2010); (2) Cool (2007); (3) Yang et al. (2007); (4) Kopparapu et al. (2008); (5) Kochanek et al. (2012).

#### A.1.31. PGC 32862

PGC 32862 is part of a group of spiral galaxies at approximately the same velocity (Figure 18 and Table 10). Our GBT H I detection at 13,969 km s<sup>-1</sup> is therefore highly likely to be contaminated, even though our measurement is in agreement with its optical velocity of 13,973 km s<sup>-1</sup> (Alam et al. 2015).

#### A.1.32. PGC 34377

The galaxy 2MASX J11164683+3039330 is 8' (or 4.5 Arcicibo beam radii) and 287 km s<sup>-1</sup> from our target, PGC 34377. It is possible, but unlikely, that our measured Arcicibo H I profile for our target is contaminated by the galaxy.

#### A.1.33. PGC 36715

There are three galaxies within 4'0 (2.2 times the Arcicibo beam size) and 46 km s<sup>-1</sup> from our target, PGC 36715: 2MASX J11462026+3543181, KUG 1143+360B, and 2MASX J11463995+3546070). It is likely that all three have contaminated our measured Arcicibo H I profile.

#### A.1.34. PGC 38333

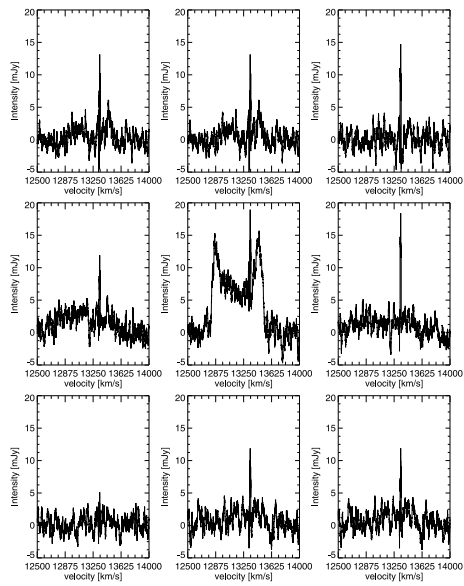
Lying within the Coma supercluster, PGC 38333 is part of a large group of galaxies, which includes a nearby companion galaxy, KUG 1203+206A, as well as NGC 4090 and a score of other galaxies, all within 15' and ±1000 km s<sup>-1</sup> of PGC 38333. Only our Arcicibo result is listed in Table 2 since, due to the smaller beam size, it is likely less contaminated by the other sources than our Nançay profile, although it is doubtful that it measured only the H I gas in our target.

#### A.1.35. PGC 38698

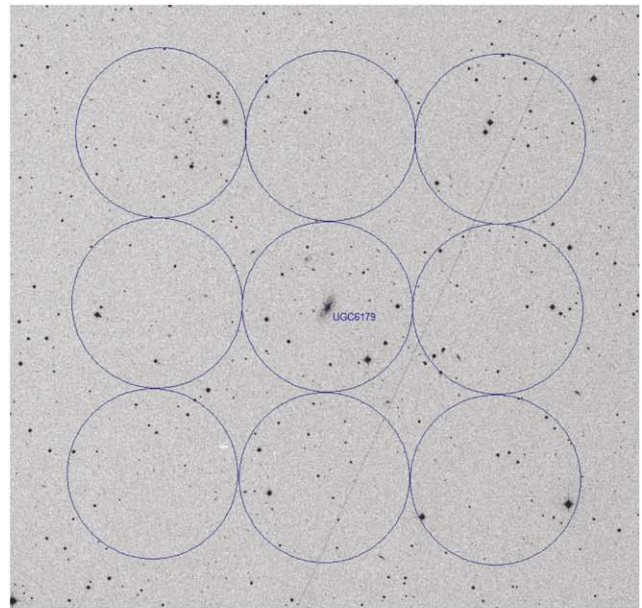
PGC 38698's morphology indicates it has recently undergone a significant interaction, most likely with its nearby companion I Zw 031, at  $V_{\text{opt}} = 6998 \text{ km s}^{-1}$  (Figure 19), as all other nearby galaxies have velocities >5000 km s<sup>-1</sup> away from I Zw 031 and PGC 38698. However, as the Nançay and GBT H I profile parameters are very similar, it is likely that all the detected H I emission is associated with our target, but it is also likely to be greatly disturbed due to a recent interaction.

#### A.1.36. PGC 38958

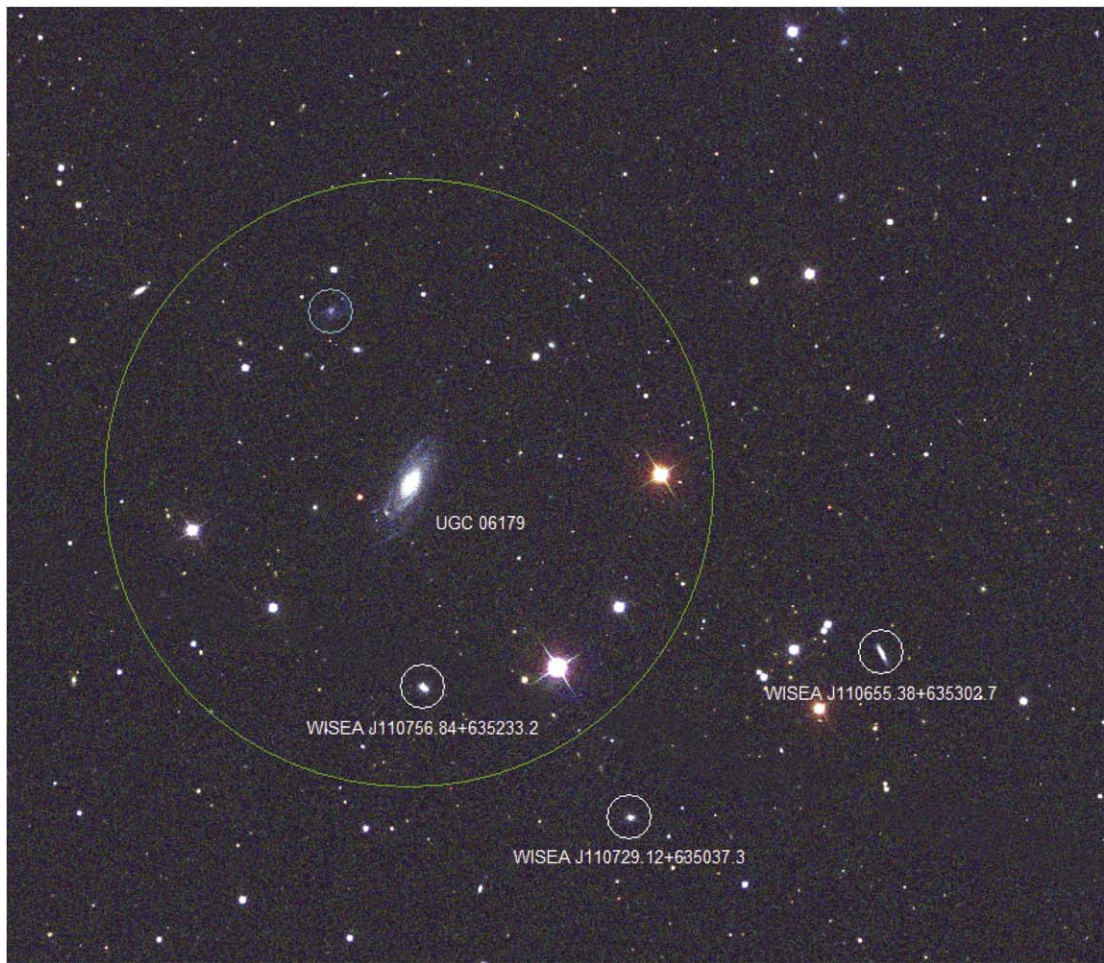
The Arcicibo ALFALFA survey reported a velocity of 5909 km s<sup>-1</sup> (Haynes et al. 2018) for PGC 38958, significantly different from the  $818 \pm 5 \text{ km s}^{-1}$  we found at Arcicibo. To explore this discrepancy further, we made very deep GBT observations of PGC 38958 but did not detect a source at 5909 km s<sup>-1</sup>, with an rms of 0.62 mJy, well below the ~8 mJy (~3.5σ) H I peaks found by ALFALFA. It is therefore highly likely the ALFALFA detection is spurious. There is no other galaxy with a known redshift within 4000 km s<sup>-1</sup> and two beamwidths of our GBT detection.



(a)



(b)



(c)

**Figure 24.** GBT observations made in a grid around UGC 6179, which indicate that the measured H I gas lies within the central beam. (a) H I spectra measured in each of the the nine 8'7 GBT beams. Please note that the ubiquitous strong, narrow line at  $\sim 13,340 \text{ km s}^{-1}$  is due to RFI. (b) Optical DSS2 blue (Abazajian et al. 2004) image with the nine GBT beams overlaid. (c) SDSS DR12 (Alam et al. 2015) false color (*i*, *r*, and *g* filters) image of UGC 6179 showing the 8' 7 GBT beam (green circle) and four known neighbors. The three galaxies with velocities near that of IC 06170 are denoted by white, labeled circles, and the previously unidentified LSB galaxy, [OVS23] 110809.3+635806, is denoted by the cyan circle.



**Table 12**  
Galaxies Likely Misidentified as Separate from UGC 6369

Object	Velocity ( $\text{km s}^{-1}$ )	Vel. References
MCG +10-16-124	1774	(1)
NGC 3625	1944	(2)
UGC 6344	1952	(3)
PGC1 0034566	2045	(1)
SBS 1118+578B	2173	(4)

**Note.** Velocity references: (1) Albareti et al. (2017); (2) Springob et al. (2005); (3) Courtois & Tully (2015); (4) Bilicki et al. (2014).

#### A.1.37. PGC 39701

There is a large group of galaxies, including IC 3157, which lie  $5'.0\text{--}8'.9$  (1.1–2.0 times the GBT beam radius) away from PGC 39701, but their velocities ( $17,511\text{--}17,921 \text{ km s}^{-1}$ ) are  $850\text{--}1250 \text{ km s}^{-1}$  lower than that of PGC 39701, at  $V_{\text{HI}} = 18,768 \text{ km s}^{-1}$ . It is possible, but unlikely, that our GBT detection is contaminated by that galaxy group.

#### A.1.38. PGC 43880

PGC 43880 is part of a group of at least four galaxies at similar velocities. One of these, SDSS J125405.61+481534.9, could in fact be considered part of our target galaxy PGC 43880 and it is surprising the SDSS survey identified it separately. The other two galaxies, WISEA J125341.21+481813.1 and WISEA J125257.97+481417.6, lie outside the GBT beam but still could be contaminating the HI profile (Figure 20). Nonetheless it is likely the measured HI emission is primarily from our target.

#### A.1.39. PGC 51872

PGC 51872 appears to be part of a loose group of galaxies (Figure 21 and Table 11). Although the various databases show a few objects within  $1000 \text{ km s}^{-1}$  from our measured velocity and within the Arecibo beam, most of these appear to be parts of our target galaxy PGC 51872, which appears to be undergoing a significant disruptive event, rather than separate galaxies.

#### A.1.40. PGC 56738

The galaxy UGC 10138 is  $230 \text{ km s}^{-1}$  and  $9'.5$  from our target, PGC 56738. Both were observed at Arecibo (see also Springob et al. 2005), and their separation is 5 times the telescope beam radius. UGC 10138 has  $V_{\text{HI}} = 9645 \text{ km s}^{-1}$ ,  $W_{50} = 685 \text{ km s}^{-1}$ , and  $F_{\text{HI}} = 1.1 \text{ Jy km s}^{-1}$ . It is unlikely it has contaminated our measured Arecibo HI flux of our target. However, UGC 10138 lies within the Nançay telescope beam and our spectrum of PGC 56738 does appear contamination by it. Therefore, only the Arecibo result is listed in Table 2.

#### A.1.41. PGC 60396

We detected an HI profile centered at  $7915 \text{ km s}^{-1}$  when pointing at PGC 60396 with the GBT. The galaxy has no published redshift and no known companions within  $15'.0$  and  $8000 \text{ km s}^{-1}$  around our GBT velocity, yet our HI profile shows a clear asymmetry. There is, though, a nearby companion, PGC 60394, which lies only  $1'.2$  away but which

has an unknown velocity. It is highly likely that we have detected both objects—PGC 60396 at  $7915 \text{ km s}^{-1}$  and PGC 60394 near  $7800 \text{ km s}^{-1}$ .

#### A.1.42. PGC 65750

PGC 65750 has two neighbors, LEDA 888740,  $13'.1$  and  $142 \text{ km s}^{-1}$  away, and LEDA 3320352,  $11'.2$  and  $1172 \text{ km s}^{-1}$  away. It is highly unlikely that either of these objects are contributing to the HI we detected at the GBT when pointing toward PGC 65750. As a result, while the optical morphology and lopsided HI profile of PGC 65750 indicate a disturbed morphology, our gas detection appears to be wholly a part of the intended target, PGC 65750.

#### A.1.43. PGC 74070

The galaxy NGC 798 is  $9'.5$  and  $351 \text{ km s}^{-1}$  away from our target, PGC 74070. It is possible that our Nançay data are slightly contaminated by NGC 798's gas, as its distance from our target is 2.5 times the Nançay beam radius, and as the smaller Arecibo beam detected a somewhat smaller flux. If that is not the case, then the HI distribution of PGC 74070 must extend beyond the  $3'.6$  Arecibo beam. Both the Nançay and Arecibo observations are included in Table 2.

#### A.1.44. PGC 77473

Our Nançay detection at  $8085 \text{ km s}^{-1}$  matches the Parkes' HIPASS and HIZOA HI velocities of source HIPASS J0730-28 (Meyer et al. 2004; Staveley-Smith et al. 2016), whose optical counterpart is identified as 2MASX J07304535-282358 by Doyle et al. (2005).

#### A.1.45. PGC 82395

The galaxy 2MASX J09262444+3304090 is  $4'.7$  (2.6 times the Arecibo beam radius) and  $67 \text{ km s}^{-1}$  from our target, PGC 82395. It is possible, but not likely, that it contaminates our Arecibo HI profile of our target.

#### A.1.46. PGC 82550

As the Arecibo observations of PGC 82550 have RFI at their edge, only the Nançay observations were used for our results in Table 2.

#### A.1.47. PGC 85851

The galaxies SDSS J235205.07+144047.2 and KUG 2349+134A are within  $4'.0$  (2.2 times the Arecibo beam radius), and  $28 \text{ km s}^{-1}$  from the measured HI velocity of our target, PGC 85851. It is highly likely that the HI flux we measured at Arecibo has been contaminated by these two other galaxies.

#### A.1.48. PGC 86863

Only the significantly higher S/N Arecibo observations were used for line profile parameter measurements in Table 2.

#### A.1.49. PGC 86903

PGC 86903 lies within a large group of galaxies. However, none of the other galaxies lie within a  $5'$  distance. It is therefore unlikely that the HI flux we measured is contaminated by another source.

*A.1.50. PGC 89535*

2MASS (Bilicki et al. 2014) lists a photometric redshift of  $11,900 \pm 4500 \text{ km s}^{-1}$  for our target PGC 89535, which is consistent with our HI value of  $13,387 \text{ km s}^{-1}$ . Otherwise, our target has no known neighbors both within the GBT beam and within  $1000 \text{ km s}^{-1}$  of its HI velocity. It is likely this is an isolated LSB galaxy.

*A.1.51. PGC 89614*

Our detection listed as PGC 89614 is more likely to be KUG 1228+248, a galaxy only  $0'.85$  from it and with an optical velocity of  $20,099 \text{ km s}^{-1}$  (Albareti et al. 2017), only  $14 \text{ km s}^{-1}$  from the velocity we found at Arecibo.

*A.1.52. PGC 91198*

The galaxy SDSS J122526.1+360102.5 is  $8'.1$  (4.5 times the Arecibo beam radius) and  $200 \text{ km s}^{-1}$  away from our target, PGC 91198. It is therefore unlikely that it is significantly contaminating our Arecibo HI profile of PGC 91198.

*A.1.53. PGC 91549*

The galaxy SDSS J164503.80+304802.1 is  $10'.4$  (4.4 times the Arecibo beam radius) and  $59 \text{ km s}^{-1}$  from our target, PGC 91549. It is therefore highly unlikely that it is contributing an appreciable amount of flux to our Arecibo HI profile of our target.

*A.1.54. PGC 95598*

PGC 95598 is part of the NGC 2273 group of galaxies, shown in Figure 22 (e.g., Tully & Fisher 1988; Gourgoulhon et al. 1992; Garcia 1993). As its nearest neighbor, NGC 2273B, lies  $11'.7$  (2.7 times the GBT beam radius) and  $307 \text{ km s}^{-1}$  away it is possible that it is contaminating our GBT HI profile.

*A.1.55. PGC 135624*

Three galaxies (NGC 391, 2MASX J01072342+0053341, and 2MASX J01073154+0053232) are all within  $7'.1$  and  $180 \text{ km s}^{-1}$  of our target PGC 135624, and within the Nançay beam. All three are likely to have added to the HI flux of our target we measured at Nançay, although we note that our profile is rather narrow ( $W_{50} = 95 \text{ km s}^{-1}$ ).

*A.1.56. PGC 135894*

Our target PGC 135894 is in a group of at least four galaxies, three of which lie within  $9'.0$  and  $1000 \text{ km s}^{-1}$  of it—WISEA J233406.20+001311.8, DEEP2 33029695, and DEEP2 33029720. Furthermore, the HI flux we measured at Nançay is 40% ( $1.5\sigma$ ) higher than at Arecibo, while the GBT flux lies between the two. It is therefore highly likely our HI measurements of PGC 135894 are contaminated by its companions. Please note that the Nançay spectrum is not shown in Figure 1.

*A.1.57. PGC 166523*

There are two galaxies, WISEA J175425.16-020235.5 and WISEA J175423.40-020032.4, which lie within  $3'$  and  $1000 \text{ km s}^{-1}$  of our target, PGC 166523. It is highly likely that the

HI profile we measured at Nançay is contaminated by these two other galaxies.

*A.1.58. PGC 2815809*

The galaxy HIPASS J0756-26 is  $6'.8$  and  $36 \text{ km s}^{-1}$  from our target, PGC 2815809. As HIPASS J0756-26 is an HI-detected galaxy only, with no optical counterpart (Doyle et al. 2005), it is likely that HIPASS J0756-26 and PGC 2815809 are the same source. However some observed HI properties of both sources differ significantly, as measured at Parkes by Meyer et al. (2004) and at Nançay and the GBT for this paper, with the HIPASS results having a 50% larger  $W_{50}$  and  $2\times$  higher flux than measured by us (PGC 2815809:  $V_{\text{HI}} = 6645 \text{ km s}^{-1}$ ,  $W_{50} = 127 \text{ km s}^{-1}$ , and  $M_{\text{HI}} = 7.5 \times 10^9 M_{\odot}$ ; HIPASS J0756-26:  $V_{\text{HI}} = 6681 \text{ km s}^{-1}$ ,  $W_{50} = 166 \text{ km s}^{-1}$ , and  $M_{\text{HI}} = 1.7 \times 10^{10} M_{\odot}$ ). Follow-up observations to determine the true HI properties of this galaxy are needed—to determine if PGC 2815809 and HIPASS J0756-26 are in fact the same source and, if so, where its center lies.

Please note that an Effelsberg HI detection was reported at a much lower velocity of  $241 \text{ km s}^{-1}$  by Huchtmeier et al. (2001), with  $W_{50} = 26 \text{ km s}^{-1}$  and  $F_{\text{HI}} = 0.7 \text{ Jy km s}^{-1}$ . Our Nançay and GBT data show no sign of this profile, however, which should have been detected at the  $S/N = 10$  level, if real. We therefore conclude the Effelsberg signal is due to Galactic HI. The Effelsberg velocity search range ends at  $4000 \text{ km s}^{-1}$ , which excludes the profile we detected.

*A.1.59. UGC 605*

UGC 605 is among our most distant detections, at  $19,536 \pm 21 \text{ km s}^{-1}$ , which matches the optical value of  $19,602 \text{ km s}^{-1}$  reported by Wang et al. (2018). The HI velocity width and gas mass we measure toward UGC 605 are both well beyond what would be expected for an individual galaxy. The mean velocities of our Arecibo and GBT profiles are the same within the uncertainties, but the Arecibo line widths and integrated line fluxes are significantly smaller than those measured with the GBT:  $W_{50} = 723$  and  $916 \text{ km s}^{-1}$ , and  $F_{\text{HI}} = 2.3$  and  $7.5 \text{ Jy km s}^{-1}$ , respectively. Within the GBT and Arecibo beams there is another galaxy (MCG +04-03-027) which lies only  $1'.3$  away, at a photometric redshift of  $26,490 \text{ km s}^{-1}$  (Bilicki et al. 2014). As this is not a precise spectroscopic velocity, it is possible that gas from this object is also contained within the our HI spectra. However, a more likely scenario is that UGC 605 is part of a loose group of interacting galaxies, which includes at least MCG +04-03-027, and two other, previously unidentified LSB galaxies shown in Figure 23 (OVS 005846.3+222221 & OVS 005813.0+221827), and possibly even the more distant galaxies WISEA J005908.02+222556.6 ( $23,919 \text{ km s}^{-1}$ ; distance to UGC 605 is  $10'.8$ ), WISEA J005852.84+22005557.4 ( $17,691 \text{ km s}^{-1}$ ; at  $13'.9$ ), and WISEA J005908.02+222556.6 ( $23,919 \text{ km s}^{-1}$ ; at  $10'.8$ ; Bilicki et al. 2014). This would also explain the notable differences in line widths and HI fluxes found between the GBT and Arecibo observations. As the Arecibo beam is the smallest, only its values are used in Table 2.

*A.1.60. UGC 1127*

We first observed UGC 1127 as part of the the UGC sample and did not detect it, to an rms of  $2.7 \text{ km s}^{-1}$ . Deeper follow-up

observations with the GBT found a clear line signal at  $20,820 \text{ km s}^{-1}$ .

#### A.1.61. UGC 1145

Our original Nançay detection showed an HI velocity at  $5784 \pm 13 \text{ km s}^{-1}$ ,  $108 \text{ km s}^{-1}$  higher than the optical value of  $5676 \pm 10 \text{ km s}^{-1}$  (Huchra et al. 2012). The Nançay detection shows a single, narrow peak around  $5690 \text{ km s}^{-1}$ , somewhat off-center amidst an about  $290 \text{ km s}^{-1}$  wide, weaker plateau. The velocity of the peak corresponds well to the optical value. As the noise level of the Nançay detection was quite high, significantly more sensitive GBT observations were taken at a later date. The GBT data confirmed the narrow peak, albeit at a lower peak value, which lies at the optical velocity, but did not confirm the wide plateau. As a result, only the GBT data were used in Table 2, although both results are shown in Figure 1 and Table 3.

#### A.1.62. UGC 1216

UGC 1216 was detected twice at Nançay, in the velocity overlap region between our searches at low and high velocities. The difference in center velocity is  $23 \text{ km s}^{-1}$ , or almost  $4\sigma$ . The line widths and line fluxes are the same within the uncertainties. The two results are listed separately in Table 3.

#### A.1.63. UGC 1851

UGC 1851 was observed a total of four times—once (using Nançay) for the UGC survey (and not detected), once at Nançay for the HyperLeda sample, and then twice with the GBT. The second set of GBT observations was made due to discrepancies between the earlier Nançay detection and GBT observations. As the new GBT values lie in between the Nançay detection and previous GBT values, the three individual detections were averaged for Table 2.

#### A.1.64. UGC 1927

UGC 1927 was part of the UGC sample but not detected at Nançay. Follow-up observations with the GBT detected the object at  $6280 \text{ km s}^{-1}$ .

#### A.1.65. UGC 2036

Our Nançay detection ( $V_{\text{HI}} = 5021 \text{ km s}^{-1}$ ,  $W_{50} = 135 \text{ km s}^{-1}$ , and  $F_{\text{HI}} = 3.6 \text{ Jy km s}^{-1}$ ) may be confused by CGCG 539-044, a highly inclined  $B_T = 15.2$  galaxy  $8/2 \text{ s}$  away from UGC 2036, with an optical velocity of  $4920 \pm 33 \text{ km s}^{-1}$  (Huchra et al. 1999).

#### A.1.66. UGC 2068

Our Nançay detection is contaminated by other galaxies within the telescope beam. UGC 2068 was detected previously in HI at Nançay by Theureau et al. (1998) at  $V_{\text{HI}} = 5740 \text{ km s}^{-1}$ ; it has no other published redshift. Our HI profile ( $V_{\text{HI}} = 5628 \text{ km s}^{-1}$ ,  $W_{50} = 586 \text{ km s}^{-1}$ , and  $F_{\text{HI}} = 7.7 \text{ Jy km s}^{-1}$ ) is very wide and has a complex structure, due to the presence of other galaxies in the beam, notably NGC 980 and NGC 982. NGC 980 is a  $B_T = 14.2 \text{ mag}$  S0 galaxy at  $V_{\text{opt}} = 5796 \pm 42 \text{ km s}^{-1}$ ,  $2/5 \text{ N}$  of our target UGC 2068, and NGC 982 is a  $B_T = 13.2 \text{ mag}$  Sa galaxy at  $V_{\text{opt}} = 5845 \pm 58 \text{ km s}^{-1}$ ,  $1/5 \text{ s}$  from our target. The HI profiles of NGC 980 and

NGC 982 measured with the  $3/6$  Arecibo beam by Magri (1994) and Haynes et al. (1988) show  $V_{\text{HI}} = 5757 \pm 9 \text{ km s}^{-1}$ ,  $W_{50} = 702 \text{ km s}^{-1}$ , and  $F_{\text{HI}} = 8.1 \text{ Jy km s}^{-1}$ , and  $V_{\text{HI}} = 5737 \pm 11 \text{ km s}^{-1}$ ,  $W_{50} = 568 \text{ km s}^{-1}$ , and  $F_{\text{HI}} = 6.9 \text{ Jy km s}^{-1}$ , respectively. As the separation between the centers of NGC 980 and 982 is  $3/6$ , all measured HI profiles are bound to be confused and therefore no conclusion can be drawn on the HI profile parameters of UGC 2068.

#### A.1.67. UGC 2113

UGC 2113 was part of the UGC sample but not detected at Nançay. Follow-up observations with the GBT detected the object at  $12,831 \text{ km s}^{-1}$ .

#### A.1.68. UGC 2139

UGC 2139 was part of the UGC sample but not detected at Nançay. Follow-up observations with the GBT detected the object at  $5113 \text{ km s}^{-1}$ .

#### A.1.69. UGC 2235

UGC 2235 was detected at Nançay in both surveys. Both sets of HI profile parameters are consistent within the uncertainties, but it is highly likely that (most of) the HI flux we detected toward UGC 2235 at  $5583 \text{ km s}^{-1}$  is associated with UGC 2234, which lies just within the Nançay HPBW. UGC 2235 has no optical velocity, whereas that of UGC 2234 is  $5562 \pm 25 \text{ km s}^{-1}$  (Huchra et al. 1999). A Nançay profile measured toward UGC 2234 by Theureau et al. (1998) shows  $V_{\text{HI}} = 5606 \text{ km s}^{-1}$ ,  $W_{50} = 267 \text{ km s}^{-1}$ , and  $F_{\text{HI}} = 3.5 \text{ Jy km s}^{-1}$ . Follow-up observations with the GBT clearly detected UGC 2234 but not UGC 2235, to the  $1.01 \text{ mJy rms}$  level.

#### A.1.70. UGC 2301 & UGC 2305

Pointing toward UGC 2301, at Nançay we detected two galaxy HI profiles, centered at  $1746 \text{ km s}^{-1}$  and  $5414 \text{ km s}^{-1}$ , respectively. We assume the former to be of our target UGC 2301 and the latter of nearby UGC 2305, a  $B_T = 16.1 \text{ SBc}$  spiral  $11/7$  south of our target. Taking into account the beam attenuation, our profile parameters of UGC 2305 ( $V_{\text{HI}} = 5414 \text{ km s}^{-1}$ ,  $W_{50} = 188 \text{ km s}^{-1}$ , and  $F_{\text{HI}} = 3.0 \text{ Jy km s}^{-1}$ ) match the mean of those measured at Nançay by Theureau et al. (1998) and at Arecibo by Wegner et al. (1993):  $V_{\text{HI}} = 5409 \text{ km s}^{-1}$ ,  $W_{50} = 189 \text{ km s}^{-1}$ , and  $F_{\text{HI}} = 4.7 \text{ Jy km s}^{-1}$ . Please note that our NRT spectrum of UGC 2305 is not shown in Figure 1.

#### A.1.71. UGC 2480

The galaxy UGC 2472 lies  $7/7$  ( $4.3$  and  $1.8$  times the Arecibo and GBT beam radii, respectively) from our target UGC 2480 and has an HI velocity of  $10,157 \text{ km s}^{-1}$  (e.g., Haynes et al. 2018),  $27 \text{ km s}^{-1}$  higher than what we measured for our target, UGC 2480. The larger  $F_{\text{HI}}$  and  $W_{20}$  values we found at the GBT, compared to Arecibo, makes it likely that our GBT data, at least, are affected by UGC 2472's proximity. As a result, only the Arecibo data are used in Table 2.

#### A.1.72. UGC 2505

The galaxy 2MASX J03034116-0104249 is  $10/4$  and  $135 \text{ km s}^{-1}$  from our target, UGC 2505. As no difference in flux is

found between the Nançay and GBT observations, though, it is unlikely that flux from 2MASX J03034116-0104249 has contaminated the profile parameters we measured for UGC 2505. GBT follow-up observations were taken of UGC 2505 to confirm this, with the same result as the earlier observations.

#### A.1.73. UGC 2668

Albareti et al. (2017) gives UGC 2668 an optical velocity of  $5450 \text{ km s}^{-1}$ , yet we see no hint of a galaxy at that velocity, to an rms of 2.8 mJy. Either the object is extremely lacking in H I gas or the optical velocity is incorrect.

#### A.1.74. UGC 2749

Our Nançay H I spectrum of UGC 2749, with  $V_{\text{H I}} = 4207 \text{ km s}^{-1}$ , is very probably confused by that of the Sc type galaxy CGCG 541-011, 5'8 to the north, which has  $V_{\text{opt}} = 4253 \pm 43 \text{ km s}^{-1}$ .

#### A.1.75. UGC 2876

UGC 2876 has no published optical velocity but it has a published Arecibo H I detection, with  $V_{\text{H I}} = 5475 \text{ km s}^{-1}$ ,  $W_{50} = 200 \text{ km s}^{-1}$ , and  $F_{\text{H I}} = 1.9 \text{ Jy km s}^{-1}$  (Monnier Ragaigine et al. 2003a). However, upon inspection of the published spectrum we estimate its central peak velocity to be  $5305 \text{ km s}^{-1}$ . This matches the other values, which were obtained with both Nançay and the GBT (with two separate GBT observations).

#### A.1.76. UGC 3041

Jones et al. (2009) give an optical velocity of  $4931 \text{ km s}^{-1}$  for UGC 3041, yet we find no H I detection at that velocity to an rms of 0.81 mJy. Either this source has an extremely low H I mass or the optical velocity is incorrect.

#### A.1.77. UGC 3797

It is likely that nearby galaxy UGC 3789 has contributed flux to our measured Nançay H I spectrum. It lies  $4'3$  from our target UGC 3797, and has an optical velocity of  $3243 \pm 70 \text{ km s}^{-1}$  (Focardi et al. 1986),  $162 \text{ km s}^{-1}$  lower than that of our target ( $3405 \pm 15 \text{ km s}^{-1}$ ; Rines et al. 2000). We observed UGC 3797 at Nançay and measured  $V_{\text{H I}} = 3399 \text{ km s}^{-1}$ ,  $W_{50} = 163 \text{ km s}^{-1}$ , and  $F_{\text{H I}} = 2.9 \text{ Jy km s}^{-1}$ , whereas UGC 3798 was observed at Nançay by Theureau et al. (1998), who reported  $V_{\text{H I}} = 3325 \text{ km s}^{-1}$ ,  $W_{50} = 389 \text{ km s}^{-1}$ , and  $F_{\text{H I}} = 1.7 \text{ Jy km s}^{-1}$ . The separation between both objects is 2.5 times the beam radius.

#### A.1.78. UGC 3963

UGC 3963 was originally observed at Nançay as part of the UGC sample. Subsequently an optical redshift of 20,236  $\text{km s}^{-1}$  was reported (Huchra et al. 2012), which places it outside our Nançay search range. However, follow-up observations with the GBT which included the optical velocity still did not detect the galaxy. Only the GBT rms is listed in Table 4.

#### A.1.79. UGC 5071

Although noted as a POSS blue plate defect and as not visible on the red POSS plate in Nilson (1973), UGC 5071 is

listed as a galaxy in Paturel et al. (2000) and HyperLeda. We did not detect H I emission in its direction.

#### A.1.80. UGC 5127

Our Arecibo spectrum shows two detections, at  $4521 \text{ km s}^{-1}$  and  $5892 \text{ km s}^{-1}$ . The former is of our target UGC 5127, with  $V_{\text{opt}} = 4508 \text{ km s}^{-1}$  (Alam et al. 2015), whereas the latter detection appears to be of SDSS J093743.77+370631.3,  $1'2$  from our target with  $V_{\text{opt}} = 5894 \text{ km s}^{-1}$  (Alam et al. 2015). The data we used are for the lower velocity detection.

#### A.1.81. UGC 5293

We detected UGC 5293 at Nançay and twice with the GBT, and found  $V_{\text{H I}} = 4986 \text{ km s}^{-1}$ ,  $W_{50} = 198 \text{ km s}^{-1}$ , and  $F_{\text{H I}} = 2.4 \text{ Jy km s}^{-1}$ . The galaxy WISEA J095234.27+412207.1 lies  $7'5$  (1.6 times the GBT beam size) away and has a velocity of  $5019 \text{ km s}^{-1}$  based on spectroscopic measurements by York et al. (2000),  $33 \text{ km s}^{-1}$  higher than our H I detections. It is possible, then, that UGC 5293 and 095234.27+412207.1 are interacting companions.

#### A.1.82. UGC 5412

The intent of this survey was to detect our target, UGC 5410. A photometric redshift of  $35,120 \text{ km s}^{-1}$  was reported subsequently (e.g., Albareti et al. 2017) for our target, well outside our H I search range. However, the GBT and Nançay beams also readily covered nearby UGC 5412, whose optical spectroscopic velocity of  $9610 \text{ km s}^{-1}$  (Alam et al. 2015) corresponds to our H I detection, and the results of this spurious detection are given in Tables 2 and 3.

#### A.1.83. UGC 5613

Due to residual RFI centered on its optical velocity of  $9656 \text{ km s}^{-1}$  (Alam et al. 2015) we are unable to draw any conclusions regarding the H I line signal of this galaxy.

#### A.1.84. UGC 5983

It is highly likely that most, or all, of our measured H I flux is from nearby NGC 3432, a much larger galaxy whose center lies  $3'4$  from the position of our target, UGC 5983. The H I profiles we measured toward UGC 5983 with the GBT and NRT are significantly different. Both telescope beams include a significant portion of NGC 3432, especially at the GBT. An Arecibo measurement of NGC 3432 by Hewitt et al. (1983) shows  $V_{\text{H I}} = 608 \text{ km s}^{-1}$ ,  $W_{20} = 248 \text{ km s}^{-1}$ , and  $F_{\text{H I}} = 138 \text{ Jy km s}^{-1}$ . We measured an  $F_{\text{H I}}$  of 78 and 32  $\text{Jy km s}^{-1}$  at the GBT and NRT, respectively. Please note that the Nançay spectrum of this galaxy is not shown in Figure 1

#### A.1.85. UGC 6005

UGC 6005 was not detected in H I by Schneider et al. (1990) with an rms noise level of 8.7 mJy, which is consistent with the average line flux density level of our detection of  $F_{\text{H I}}/W_{50} = 15.5 \text{ mJy}$ .

#### A.1.86. UGC 6179

The original GBT observation, pointed at the galaxy center, showed a huge profile width ( $W_{20} = 913 \text{ km s}^{-1}$ ), total H I mass ( $\log(M_{\text{H I}}/M_{\odot}) = 10.81$ ), and  $V_{\text{H I}} = 13,155 \text{ km s}^{-1}$  in agreement



with its optical spectroscopic velocity of  $13,145 \text{ km s}^{-1}$  (Albaret et al. 2017). Confirmation observations with the GBT on a grid surrounding the galaxy indicate the detected HI mass is confined within the original GBT beam (Figure 24). A literature search shows only one other galaxy, WISEA J110756.84+635233.2, which lies within the central GBT beam and has a velocity similar to that of UGC 6179 ( $V_{\text{opt}} = 13,173 \text{ km s}^{-1}$ ). However, two more galaxies, WISEA J110655.38+635302.7 and WISEA J110729.12+635037.3, lie just outside the GBT beam at very similar velocities ( $V_{\text{opt}} = 13,061$  and  $13,117 \text{ km s}^{-1}$ , respectively). Additionally, though, inspection of images from the SDSS (Alam et al. 2015) indicates there are a number of previously unidentified galaxies within the beam. One of these, shown in Figure 24, appears to be a blue LSB galaxy, which is likely also part of the galaxy group surrounding UGC 6179. As the Nançay spectrum for this galaxy has RFI in the middle of the measured spectrum, only the GBT data are used for determining the line parameters of UGC 6179.

#### A.1.87. UGC 6369

There are at least five other galaxies within  $11'0$  and  $1000 \text{ km s}^{-1}$  of UGC 6369; see Table 12 for a list of its known neighbors. It is therefore highly likely that our Nançay HI profile of UGC 6369 is confused.

#### A.1.88. UGC 6489

UGC 6489 has two nearby neighbors—LEDA 2198942 at  $6'9$  and  $335 \text{ km s}^{-1}$  away and ASK 347484.0 at  $8'4$  and  $653 \text{ km s}^{-1}$  away (Abazajian et al. 2004; Bilicki et al. 2014). However, based both on the HI profile and morphology of UGC 6489, it is likely that the spectrum is not contaminated.

#### A.1.89. UGC 6812

Alam et al. (2015) gives an optical spectroscopic velocity for UGC 6812 of  $6785 \text{ km s}^{-1}$ , yet there is no HI detected at that velocity to a  $1\sigma$  limit of  $1.7 \text{ mJy}$ . Either the reported velocity is incorrect or UGC 6182 has a very-low HI mass.

#### A.1.90. UGC 7146

We detected UGC 7953 at  $17,211 \text{ km s}^{-1}$  with the GBT, whereas the SDSS DR12 (Alam et al. 2015) reported an optical velocity of  $1093 \pm 14 \text{ km s}^{-1}$ . However, as the SDSS classified the spectrum as “star F9” and it shows no emission lines, it is likely that the reported velocity is erroneous. Furthermore, our GBT and Arecibo observations did not detect HI at the  $1093$  velocity. However numerous other HI studies have found velocities similar to ours, giving significant confidence in our results (e.g., Wolfinger et al. 2013; Pak et al. 2014; van Driel et al. 2016). Our target UGC 7146, is listed as a member of galaxy group [RPG97] 186 (Ramella et al. 1997), whose center position lies  $11'$  and  $216 \text{ km s}^{-1}$  from our target, but all 18 objects within  $12'$  distance with known redshifts are much more distant (at  $20,000$ – $50,000 \text{ km s}^{-1}$ ) than our nearby ( $1060 \text{ km s}^{-1}$ ) target. It therefore seems unlikely that other group members have contaminated our GBT or Nançay spectra of UGC 7146.

#### A.1.91. UGC 7553

UGC 7553 has an optical spectroscopic velocity of  $8733 \text{ km s}^{-1}$  (Colless et al. 2001). Our HI detection at Nançay, and another by Matthews & van Driel (2000), both measured a  $90$

$\text{km s}^{-1}$  higher HI velocity of  $8823 \text{ km s}^{-1}$ . Both HI spectra may be confused by nearby CGCG 014-041, a  $B_T = 14.8$  mag galaxy  $9'8$  to the north, at  $V_{\text{opt}} = 8806 \pm 35 \text{ km s}^{-1}$ , although it is not expected to be HI rich given its S0 classification.

#### A.1.92. UGC 7953

The online HI spectrum from Alam et al. (2015) has a listed velocity of  $17,192 \pm 4 \text{ km s}^{-1}$ , which is close to the  $17,211 \text{ km s}^{-1}$  we detected with the GBT. However, the Ann et al. (2015) paper on the optical spectrum reports a detection at  $1093 \text{ km s}^{-1}$ . Three other HI observations, from van Driel et al. (2016) as well as our GBT and Arecibo observations, detected nothing at that velocity. It is therefore likely that the reported detection at  $1093 \text{ km s}^{-1}$  velocity is erroneous or due to another object.

#### A.1.93. UGC 8107

Using the GBT, Masters et al. (2014) measured  $W_{50} = 747 \text{ km s}^{-1}$  toward UGC 8107, significantly larger than the  $602 \pm 34 \text{ km s}^{-1}$  we found at Nançay. Our follow-up GBT observations, though, gave an even higher value, of  $W_{50} = 988 \text{ km s}^{-1}$ . The measured HI line fluxes of all three measurement are consistent. As the S/Ns for the two GBT measurements are significantly higher than for the Nançay measurement, the GBT value is more reliable, but the measured error is high. The average of the measured values is given here.

#### A.1.94. UGC 8222

The detection of UGC 8222 is marginal, with our confidence in the detection due to Alam et al. (2015)’s earlier determination of the galaxy’s spectroscopic velocity.

#### A.1.95. UGC 8659

Given its much higher HI velocity of  $5001 \text{ km s}^{-1}$ , UGC 8659 is clearly not a member of the M101 group (mean velocity  $\sim 240 \text{ km s}^{-1}$ ), as was considered a possibility by Bremnes et al. (1999). Surface photometry in the *B* and *R* bands (Bremnes et al. 1999) shows it has an Im morphology, an extrapolated  $B_T = 16.16$  mag, a central blue disk surface brightness of  $23.2 \text{ mag arcsec}^{-2}$ , a blue disk scale length of  $11''.2$ , and an increasingly blue color with radius.

#### A.1.96. UGC 8802

UGC 8802 has two nearby galaxies, WISEA J135337.14+354117.7 at  $6'0$  and  $400 \text{ km s}^{-1}$  away from it, and CGCG 191-005 at  $8'1$  and  $329 \text{ km s}^{-1}$  away. However, as both the Nançay and Arecibo spectra look similar it is unlikely that either galaxy has contributed to the measured HI flux of UGC 8802.

#### A.1.97. UGC 9783

The SDSS optical value of  $11,168 \pm 6 \text{ km s}^{-1}$  (Albaret et al. 2017) of UGC 9783 corresponds exactly to the  $11,168 \pm 10 \text{ km s}^{-1}$  we measured in our GBT follow-up observations. Our Nançay profile is quite different (see Table 3), but as it was detected near the edge of the NRT bandpass and the rms of our GBT spectrum is five times smaller, only the GBT results are reported in Table 2.

## A.1.98. UGC 10666 and UGC 10668

Our Arecibo data show two separated profiles, centered at 9809 and 10,101 km s<sup>-1</sup>, respectively. Our target galaxy UGC 10666, has a 2MASS photometric redshift of 16,047 km s<sup>-1</sup> (Bilicki et al. 2014) whereas UGC 10668, at 2/2 separation, has an optical spectroscopic velocity of 10,162 ± 45 km s<sup>-1</sup> (Huchra et al. 2012). UGC 10668's optical velocity corresponds to the higher-velocity HI detection, although as UGC 10668 lies on the edge of the telescope beam its flux is likely underestimated by a factor of 2 or so. It is also likely that the lower measured HI velocity corresponds to UGC 10666. Our Nançay observations were not sensitive enough (rms of 3.2 mJy) to detect the profiles.

## A.1.99. UGC 11900

UGC 11900 has one neighbor, LEDA 167572, which lies 4/5 and 405 km s<sup>-1</sup> away. The standard, double-horned shape of the UGC 11900 HI profile combined with the difference in velocities of the two galaxies makes it highly unlikely that its HI profile is contaminated by its neighbor.

## ORCID iDs

K. O'Neil  <https://orcid.org/0000-0002-2502-5808>

W. van Driel  <https://orcid.org/0000-0003-4770-9829>

## References

- Abazajian, K., Adelman-McCarthy, J. K., Agüeros, M. A., et al. 2003, *AJ*, **126**, 2081
- Abazajian, K., Adelman-McCarthy, J. K., Agüeros, M. A., et al. 2004, *AJ*, **128**, 502
- Abazajian, K. N., Adelman-McCarthy, J. K., & Agüeros, M. A. 2009, *ApJS*, **182**, 543
- Adelman-McCarthy, J. K., Agüeros, M. A., Allam, S. S., et al. 2007, *ApJS*, **172**, 634
- Ahn, C. P., Alexandroff, R., Allende Prieto, C., et al. 2012, *ApJS*, **203**, 21
- Ahumada, R., Prieto, C. A., Almeida, A., et al. 2020, *ApJS*, **249**, 3
- Alam, S., Albareti, F. D., Allende Prieto, C., et al. 2015, *ApJS*, **219**, 12
- Alatalo, K., Cales, S. L., Rich, J. A., et al. 2016, *ApJS*, **224**, 38
- Albareti, F. D., Allende Prieto, C., Almeida, A., et al. 2017, *ApJS*, **233**, 25
- Ann, H. B., Seo, M., & Ha, D. K. 2015, *ApJS*, **217**, 27
- Bell, E. F., & Bower, R. G. 2000, *MNRAS*, **319**, 235
- Bellazzini, M., Beccari, G., Oosterloo, T. A., et al. 2011a, *A&A*, **527**, A58
- Bellazzini, M., Perina, S., Galletti, S., & Oosterloo, T. 2011b, *A&A*, **533**, A37
- Berlind, A. A., Frieman, J., Weinberg, D. H., et al. 2006, *ApJS*, **167**, 1
- Berrington, R. C., Lugger, P. M., & Cohn, H. N. 2002, *AJ*, **123**, 2261
- Bilicki, M., Jarrett, T. H., Peacock, J. A., Cluver, M. E., & Steward, L. 2014, *ApJS*, **210**, 9
- Bothun, G. D., Beers, T. C., Mould, J. R., & Huchra, J. P. 1985, *AJ*, **90**, 2487
- Bothun, G. D., Impey, C. D., Malin, D. F., & Mould, J. R. 1987, *AJ*, **94**, 23
- Bouchard, A., Da Costa, G. S., & Jerjen, H. 2009, *AJ*, **137**, 3038
- Bouchard, A., Jerjen, H., Da Costa, G. S., & Ott, J. 2005, *AJ*, **130**, 2058
- Bralts-Kelly, L., Bulatek, A. M., Chinski, S., et al. 2017, *ApJL*, **848**, L10
- Braun, R., Thilker, D., & Walterbos, R. A. M. 2003, *A&A*, **406**, 829
- Bremnes, T., Binggeli, B., & Prugniel, P. 1999, *A&AS*, **137**, 337
- Burkholder, V., Impey, C., & Sprayberry, D. 2001, *AJ*, **122**, 2318
- Christlein, D., & Zabludoff, A. I. 2003, *ApJ*, **591**, 764
- Clauwens, B., Schaye, J., Franx, M., & Bower, R. G. 2018, *MNRAS*, **478**, 3994
- Colless, M., Dalton, G., Maddox, S., et al. 2001, *MNRAS*, **328**, 1039
- Cool, R. J. 2007, *ApJS*, **169**, 21
- Courtois, H. M., & Tully, R. B. 2015, *MNRAS*, **447**, 1531
- Courtois, H. M., Tully, R. B., Fisher, J. R., et al. 2009, *AJ*, **138**, 1938
- Dabringhausen, J., & Fellhauer, M. 2016, *MNRAS*, **460**, 4492
- Doyle, M. T., Drinkwater, M. J., Rohde, D. J., et al. 2005, *MNRAS*, **361**, 34
- Du, W., Wu, H., Lam, M. L., et al. 2015, *AJ*, **149**, 199
- Escoffier, R. P., & Webber, J. C. 1998, *Proc. SPIE*, **3357**, 424
- Falco, E. E., Kurtz, M. J., Geller, M. J., et al. 1999, *PASP*, **111**, 438
- Focardi, P., Marano, B., & Vettolani, G. 1986, *A&A*, **161**, 217
- Galaz, G., Herrera-Camus, R., Garcia-Lambas, D., & Padilla, N. 2011, *ApJ*, **728**, 74
- Gallagher, J. S., & Bushouse, H. 1983, *AJ*, **88**, 55
- Galloway, M. A., Willett, K. W., Fortson, L. F., et al. 2015, *MNRAS*, **448**, 3442
- Garcia, A. M. 1993, *A&AS*, **100**, 47
- Geha, M., Wechsler, R. H., Mao, Y.-Y., et al. 2017, *ApJ*, **847**, 4
- Gourgoulhon, E., Chamaraux, P., & Fouque, P. 1992, *A&A*, **255**, 69
- Haynes, M. P., Giovanelli, R., Kent, B. R., et al. 2018, *ApJ*, **861**, 49
- Haynes, M. P., Giovanelli, R., Martin, A. M., et al. 2011, *AJ*, **142**, 170
- Haynes, M. P., Giovanelli, R., Starosta, B. M., & Magri, C. 1988, *AJ*, **95**, 607
- Hewitt, J. N., Haynes, M. P., & Giovanelli, R. 1983, *AJ*, **88**, 272
- Hoffman, Y., Silk, J., & Wyse, R. F. G. 1992, *ApJL*, **388**, L13
- Huang, S., Haynes, M. P., Giovanelli, R., et al. 2014, *ApJ*, **793**, 40
- Huchra, J., Davis, M., Latham, D., & Tonry, J. 1983, *ApJS*, **52**, 89
- Huchra, J. P., Macri, L. M., Masters, K. L., et al. 2012, *ApJS*, **199**, 26
- Huchra, J. P., Vogeley, M. S., & Geller, M. J. 1999, *ApJS*, **121**, 287
- Huchtmeier, W. K. 1997, *A&A*, **319**, 401
- Huchtmeier, W. K., Karachentsev, I. D., & Karachentseva, V. E. 2001, *A&A*, **377**, 801
- Impey, C., Burkholder, V., & Sprayberry, D. 2001, *AJ*, **122**, 2341
- Impey, C. D., Sprayberry, D., Irwin, M. J., & Bothun, G. D. 1996, *ApJS*, **105**, 209
- Jerjen, H., Freeman, K. C., & Binggeli, B. 1998, *AJ*, **116**, 2873
- Jones, D. H., Read, M. A., Saunders, W., et al. 2009, *MNRAS*, **399**, 683
- Jones, D. H., Saunders, W., Read, M., & Colless, M. 2005, *PASA*, **22**, 277
- Karachentsev, I. D., & Karachentseva, V. E. 1984, *Afz*, **21**, 641
- Karachentsev, I. D., Makarov, D. I., & Kaisina, E. I. 2013, *AJ*, **145**, 101
- Kazarian, M. A., & Karapetian, E. L. 2002, *Ap*, **45**, 458
- Knezek, P. M. 1993, PhD thesis, Massachusetts Univ., Amherst.
- Knezek, P. M., Sembach, K. R., Gallagher, J. S. I., et al. 1999, *ApJ*, **514**, 119
- Kochanek, C. S., Eisenstein, D. J., Cool, R. J., et al. 2012, *ApJS*, **200**, 8
- Kopparapu, R. K., Hanna, C., Kalogera, V., et al. 2008, *ApJ*, **675**, 1459
- Koribalski, B. S., Staveley-Smith, L., Kilborn, V. A., et al. 2004, *AJ*, **128**, 16
- Kormendy, J., & Westpfahl, D. J. 1989, *ApJ*, **338**, 752
- Kourkchi, E., & Tully, R. B. 2017, *ApJ*, **843**, 16
- Kozłowski, S., Kochanek, C. S., Stern, D., et al. 2010, *ApJ*, **716**, 530
- Kruk, S. J., Lintott, C. J., Bamford, S. P., et al. 2018, *MNRAS*, **473**, 4731
- Kulier, A., Galaz, G., Padilla, N. D., & Trayford, J. W. 2020, *MNRAS*, **496**, 3996
- Lang, R. H., Boyce, P. J., Kilborn, V. A., et al. 2003, *MNRAS*, **342**, 738
- Lauberts, A., & Valentijn, E. A. 1989, The Surface Photometry Catalogue of the ESO-Uppsala Galaxies (Garching: European Southern Observatory)
- Lelli, F., Fraternali, F., & Sancisi, R. 2010, *A&A*, **516**, A11
- Lutz, K. A., Kilborn, V. A., Catinella, B., et al. 2017, *MNRAS*, **467**, 1083
- Magri, C. 1994, *AJ*, **108**, 896
- Makarov, D., Prugniel, P., Terekhova, N., Courtois, H., & Vauglin, I. 2014, *A&A*, **570**, A13
- Makarov, D. I., Burenkov, A. N., & Tyurina, N. V. 2001, *AstL*, **27**, 213
- Makarov, D. I., Karachentsev, I. D., & Burenkov, A. N. 2003, *A&A*, **405**, 951
- Makarov, D. I., Karachentsev, I. D., Tyurina, N. V., & Kaisin, S. S. 1997, *AstL*, **23**, 445
- Mapelli, M., Moore, B., Ripamonti, E., et al. 2008, *MNRAS*, **383**, 1223
- Martin, G., Kaviraj, S., Laigle, C., et al. 2019, *MNRAS*, **485**, 796
- Marzke, R. O., Huchra, J. P., & Geller, M. J. 1996, *AJ*, **112**, 1803
- Masters, K. L., Crook, A., Hong, T., et al. 2014, *MNRAS*, **443**, 1044
- Matthews, L. D., & Gallagher, J. S. I. 1996, *AJ*, **111**, 1098
- Matthews, L. D., & van Driel, W. 2000, *A&AS*, **143**, 421
- Meyer, M. J., Zwaan, M. A., Webster, R. L., et al. 2004, *MNRAS*, **350**, 1195
- Mishra, A., Kantharia, N. G., Das, M., Omar, A., & Srivastava, D. C. 2017, *MNRAS*, **464**, 2741
- Monnier Ragaïne, D., van Driel, W., O'Neil, K., et al. 2003a, *A&A*, **408**, 67
- Monnier Ragaïne, D., van Driel, W., Schneider, S. E., Balkowski, C., & Jarrett, T. H. 2003b, *A&A*, **408**, 465
- Monnier Ragaïne, D., van Driel, W., Schneider, S. E., Jarrett, T. H., & Balkowski, C. 2003c, *A&A*, **405**, 99
- Moretti, A., Gullieuszik, M., Poggianti, B., et al. 2017, *A&A*, **599**, A81
- NED Team 1992, Redshift Obtained from Literature by the NED Team prior to November 1992, <http://ned.ipac.caltech.edu/uri/NED:Refcode/1992NED11.R.....1N>
- Nilson, P. 1973, Uppsala General Catalogue of Galaxies (Uppsala: Uppsala Astron. Obs)
- Oegerle, W. R., & Hill, J. M. 2001, *AJ*, **122**, 2858
- O'Neil, K., Bothun, G., van Driel, W., & Monnier Ragaïne, D. 2004, *A&A*, **428**, 823
- O'Neil, K., Bothun, G. D., & Schombert, J. 2000, *AJ*, **119**, 136

- O'Neil, K., Bothun, G. D., Schombert, J., Cornell, M. E., & Impey, C. D. 1997, *AJ*, **114**, 2448
- O'Neil, K., Oey, M. S., & Bothun, G. 2007, *AJ*, **134**, 547
- Pak, M., Rey, S.-C., Lisker, T., et al. 2014, *MNRAS*, **445**, 630
- Paturel, G., Petit, C., Garnier, R., & Prugniel, P. 2000, *A&AS*, **144**, 475
- Paturel, G., Theureau, G., Bottinelli, L., et al. 2003, *A&A*, **412**, 57
- Pickering, T. E., Impey, C. D., van Gorkom, J. H., & Bothun, G. D. 1997, *AJ*, **114**, 1858
- Prestage, R. M., Bloss, M., Brandt, J., et al. 2015, in 2015 URSI-USNC Radio Science Meeting (New York: IEEE), **4**
- Proctor, R. N., Forbes, D. A., Brodie, J. P., & Strader, J. 2008, *MNRAS*, **385**, 1709
- Ramatsoku, M., Verheijen, M. A. W., Kraan-Korteweg, R. C., et al. 2016, *MNRAS*, **460**, 923
- Ramella, M., Pisani, A., & Geller, M. J. 1997, *AJ*, **113**, 483
- Rines, K., Geller, M. J., Diaferio, A., Mohr, J. J., & Wegner, G. A. 2000, *AJ*, **120**, 2338
- Rines, K., Geller, M. J., Kurtz, M. J., & Diaferio, A. 2003, *AJ*, **126**, 2152
- Rines, K. J., Geller, M. J., Diaferio, A., & Hwang, H. S. 2016, *ApJ*, **819**, 63
- Rosenberg, J. L., & Schneider, S. E. 2002, *ApJ*, **567**, 247
- Ryan-Weber, E., Koribalski, B. S., Staveley-Smith, L., et al. 2002, *AJ*, **124**, 1954
- Saburova, A. S., Chilingarian, I. V., Kasparova, A. V., et al. 2021, *MNRAS*, **503**, 830
- Schneider, S. E., Helou, G., Salpeter, E. E., & Terzian, Y. 1986, *AJ*, **92**, 742
- Schneider, S. E., Thuan, T. X., Magri, C., & Wadiak, J. E. 1990, *ApJS*, **72**, 245
- Schneider, S. E., Thuan, T. X., Mangum, J. G., & Miller, J. 1992, *ApJS*, **81**, 5
- Schombert, J. 1998, *AJ*, **116**, 1650
- Simien, F., & Prugniel, P. 2002, *A&A*, **384**, 371
- Sprayberry, D., Impey, C. D., Bothun, G. D., & Irwin, M. J. 1995, *AJ*, **109**, 558
- Springob, C. M., Haynes, M. P., Giovanelli, R., & Kent, B. R. 2005, *ApJS*, **160**, 149
- Staveley-Smith, L., Kraan-Korteweg, R. C., Schröder, A. C., et al. 2016, *AJ*, **151**, 52
- Stetson, P. B. 1984, *PASP*, **96**, 128
- Strauss, M. A., & Davis, M. 1988, *A Redshift Survey of IRAS Galaxies*, Vol. 297 (New York: Springer), 361
- Tempel, E., Tago, E., & Liivamägi, L. J. 2012, *A&A*, **540**, A106
- Tempel, E., Tuvikene, T., Kipper, R., & Libeskind, N. I. 2017, *A&A*, **602**, A100
- Theureau, G., Bottinelli, L., Coudreau-Durand, N., et al. 1998, *A&AS*, **130**, 333
- Theureau, G., Coudreau, N., Hallet, N., et al. 2005, *A&A*, **430**, 373
- Tully, R. B., & Fisher, J. R. 1988, *Catalog of Nearby Galaxies* (Cambridge: Cambridge Univ. Press)
- Tully, R. B., & Fouque, P. 1985, *ApJS*, **58**, 67
- van den Hoek, L. B., de Blok, W. J. G., van der Hulst, J. M., & de Jong, T. 2000, *A&A*, **357**, 397
- van Driel, W., Arnaboldi, M., Combes, F., & Sparke, L. S. 2000, *A&AS*, **141**, 385
- van Driel, W., Butcher, Z., Schneider, S., et al. 2016, *A&A*, **595**, A118
- Véron-Cetty, M. P., Joly, M., Véron, P., et al. 2006, *A&A*, **451**, 851
- Wang, L.-L., Luo, A. L., Shen, S.-Y., et al. 2018, *MNRAS*, **474**, 1873
- Warren, B. E., Jerjen, H., & Koribalski, B. S. 2007, *AJ*, **134**, 1849
- Wegner, G., Haynes, M. P., & Giovanelli, R. 1993, *AJ*, **105**, 1251
- Wolfinger, K., Kilborn, V. A., Koribalski, B. S., et al. 2013, *MNRAS*, **428**, 1790
- Yang, X., Mo, H. J., van den Bosch, F. C., et al. 2007, *ApJ*, **671**, 153
- York, D. G., Adelman, J., Anderson, J. E., Jr., et al. 2000, *AJ*, **120**, 1579
- Zabludoff, A. I., & Mulchaey, J. S. 1998, *ApJ*, **496**, 39
- Zavala, J., Frenk, C. S., Bower, R., et al. 2016, *MNRAS*, **460**, 4466
- Zwaan, M. A., Meyer, M. J., Webster, R. L., et al. 2004, *MNRAS*, **350**, 1210